Supporting Information for

The Key Role of the Latent N-H Group in Milstein's Catalyst for Ester Hydrogenation

John Pham, Cole E. Jarczyk, Eamon F. Reynolds, Sophie. E. Kelly, Thao Kim, Tianyi He, Jason M. Keith*, and Anthony R. Chianese*

Table of Contents

General Methods. Unless stated otherwise, all reactions were assembled in an argon-filled MBraun Labmaster 130 glovebox. Solvents were purchased in anhydrous form from EMD-Millipore or Acros and were deoxygenated by sparging with argon before bringing into the glovebox. All reagents and materials were commercially available and were used as received, unless otherwise noted. Because of the known ability of minor carboxylic acid impurities in esters to inhibit catalysts for ester hydrogenation,[1] hexyl

hexanoate was purified by column chromatography on silica gel, eluting with 5% MTBE in hexanes, before sparging with argon and bringing into the glovebox. Hydrogen gas was purchased from Airgas at the Ultrahigh Purity level. NMR spectra were recorded at room temperature unless otherwise noted on a Bruker spectrometer (400.13 MHz for ^{1}H and 100.62 MHz for ^{13}C, 161.97 MHz for ^{31}P) and referenced to the residual solvent resonance (δ in parts per million, J in Hz). NMR assignments were made on the basis of COSY, NOESY, HSQC, and HMBC spectra, which are included as images in this document. Gas chromatography was conducted using a Shimadzu 2030 system equipped with an FID detector. Elemental analyses were performed by Robertson Microlit, Madison, NJ.

Computational Methods. Density functional theory calculations were performed using the Gaussian 16 computational chemistry package, Revision B.01.[2] The geometries and energies of all species were calculated using the hybrid functional B3LYP,[3] augmented with the addition of empirical dispersion with Grimme's D3 dispersion corrections[3] (referred to as B3LYP-D3). Ru was modeled with the effective core potential of Hay and Wadt[4] and the accompanying uncontracted basis set (including f polarization functions)[5] collectively known as LANL08(f).[6] All other elements were modeled with the 6-311G(d,p) basis set.[7] A superfine integration grid was used for all calculations, which aided convergence of structures with loosely bound fragments such as explicit ethanol molecules. Complete structures with no truncations were used in all cases. Geometry optimization and frequency calculation were conducted in solvent, using a polarizable continuum with radii and non-electrostatic terms from Truhlar and coworkers' SMD solvation model, and with dielectric constants chosen for toluene.[8] Geometry optimization in solvent is important to identify ion-pair intermediates that might be missed in the gas phase.[9] However, some weakly bound intermediates (especially H_2 and C-H σ-complexes) and two transition states failed to converge in solvent. In these difficult cases, we repeated the calculations using different, nearly converged starting points, each time with a fresh calculation of the force constants, using a range of values for the maximum step size. Despite this effort, convergence in solvent was not successful for **j**, **eP**, **eP-eq**, **eN1-eq**, **eN1**, **eN1-g1-TS**, **eN1s**, **gP2-eq**, **gP2**, and **i1-p1-TS**. For these structures, the geometry optimization and frequency calculation used for free-energy corrections were done in the gas phase at the same B3LYP-D3/6-311G(d,p)/LANL08(f) level described above, then a single-point electronic-energy refinement at the M06/6-311+G(2d,2p)/LANL08(f) level was conducted using the solvent model.

Frequency calculations ensured the absence of imaginary vibrational modes in intermediates and the presence of exactly one imaginary mode in transition states. Intrinsic reaction coordinate calculations were employed to verify that transition states led to the specified minima. For the transition states **a2-b2-TS**, **c2-d2-TS**, **i-j-TS**, **m-n-TS**, **s-t-TS**, **hd-id-TS**, **id-jd-TS**, and **od-pd-TS**, one or both connected intermediates were calculated to be higher in free energy than the transition state, an outcome which is unusual but well-precedented.[10] In each case, the energy of the intermediate was lower than the transition state on the solvent-corrected B3LYP-D3 electronic energy surface employed for geometry optimization. Standard state corrections were added in order to adjust from 1 atm to 1 M for solution-phase free energies, amounting to 1.89 kcal/mol added to the free energy of each isolated molecule at 298.15 K.[11] Although the standard state for molecular hydrogen is sometimes taken as the gas at 1 atm, we have used a 1 M standard state in toluene, for consistency in computing reaction kinetics from the calculated free energies. The solvation-corrected electronic energies were further refined using the M06 functional,[12] using the same LANL08(f) basis set for ruthenium and 6-311+G(2d,2p) for all other atoms. All energies reported in the paper are

standard-state free energies at 298.15 K. A table of energies is provided in the Supporting Information, and geometries in Cartesian coordinates are included in a separate, compiled .XYZ file.

Alternative Pathways for Hydrogen Activation. Figure 1 in the main text shows our calculated minimum-energy pathway (MEP) for hydrogen activation. We also located a direct pathway connecting **a2** to **d2**, where the Ru-bound ethoxide dissociates and deprotonates the outer-sphere ethanol molecule in a concerted manner through **a2-d2-TS** (Figure S1). This direct pathway, which keeps the N-H bond intact for the entire H_2-activation sequence, has a slightly higher barrier of 14.1 kcal/mol as compared to 12.9 kcal/mol in the Figure 1 pathway.

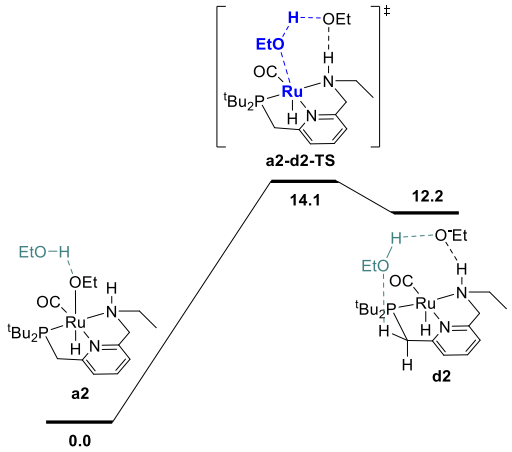

Figure S1. Alternate pathway to convert hydrido-ethoxide **a2** into unsaturated intermediate **d2**, by direct dissociation of the ethoxide ligand without prior deprotonation of nitrogen. As in the main text, all numbers given are free energies at 298.15 K, using a 1 M standard state for all species, and referenced against the resting state **a2** and the organic reactants ethyl acetate and two molecules of hydrogen. In transition states, atoms participating in bond-forming or bond-cleaving events are highlighted in **bold and blue**. In intermediates and transition states, ethanol molecules interacting only through hydrogen bonds or dative bonds are turquoise. Small molecules entering or leaving the sequence are in **red**.

In the MEP featured in Figure 1 in the main text, nitrogen is protonated prior to H-H cleavage in the conversion of **c2** to **f2**. We also identified a pathway where hydrogen coordination precedes reprotonation of nitrogen, which proceeds through a higher barrier of 15.2 kcal/mol (Figure S2).

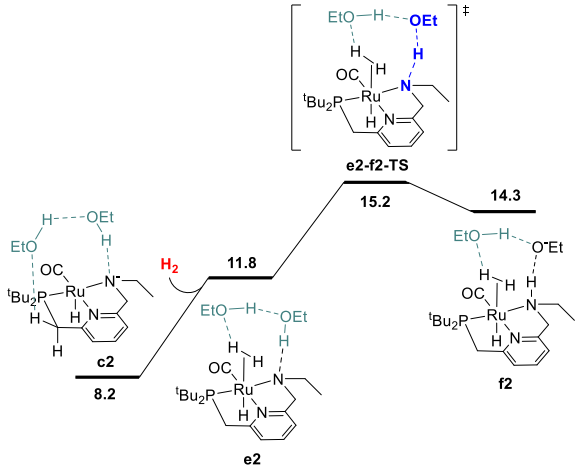

Figure S2. Alternate pathway to convert unsaturated intermediate **c2** into dihydrogen complex **f2**, where dihydrogen coordination to give **e2** precedes protonation of nitrogen to give **f2**.

In addition to the "proton-brigade" MEP described in Figure 1 of the main text including two explicit ethanol molecules, we calculated analogous pathways proceeding via cooperativity of the N-H group, which included one or zero ethanol molecules as proton shuttle. Both pathways are shown in Figure S3, and share the common path from the resting state **a2** to dissociate ethanol giving **c1**. Along this sequence, **a2** loses an ethanol molecule to give **a1**, which dissociates ethoxide and transfers the proton from N to O in a concerted transition state **a1-b1-TS** giving **b1**. The neutral ethanol oxygen then completely dissociates from Ru giving the hydrogen-bonded unsaturated intermediate **c1**. If the ethanol remains, hydrogen coordinates giving **e1**, and is activated in the concerted proton-shuttle transition state **e1-g1-TS**, to give the dihydride **g1**. In this pathway, the overall barrier is 18.6 kcal/mol, compared with 15.0 in the two-ethanol pathway in Figure 1. If instead, a second ethanol molecule fully dissociates from **c1** giving **c**, then hydrogen activation proceeds through the higher-energy transition state **e-g-TS**, with a barrier of 25.3 kcal/mol.

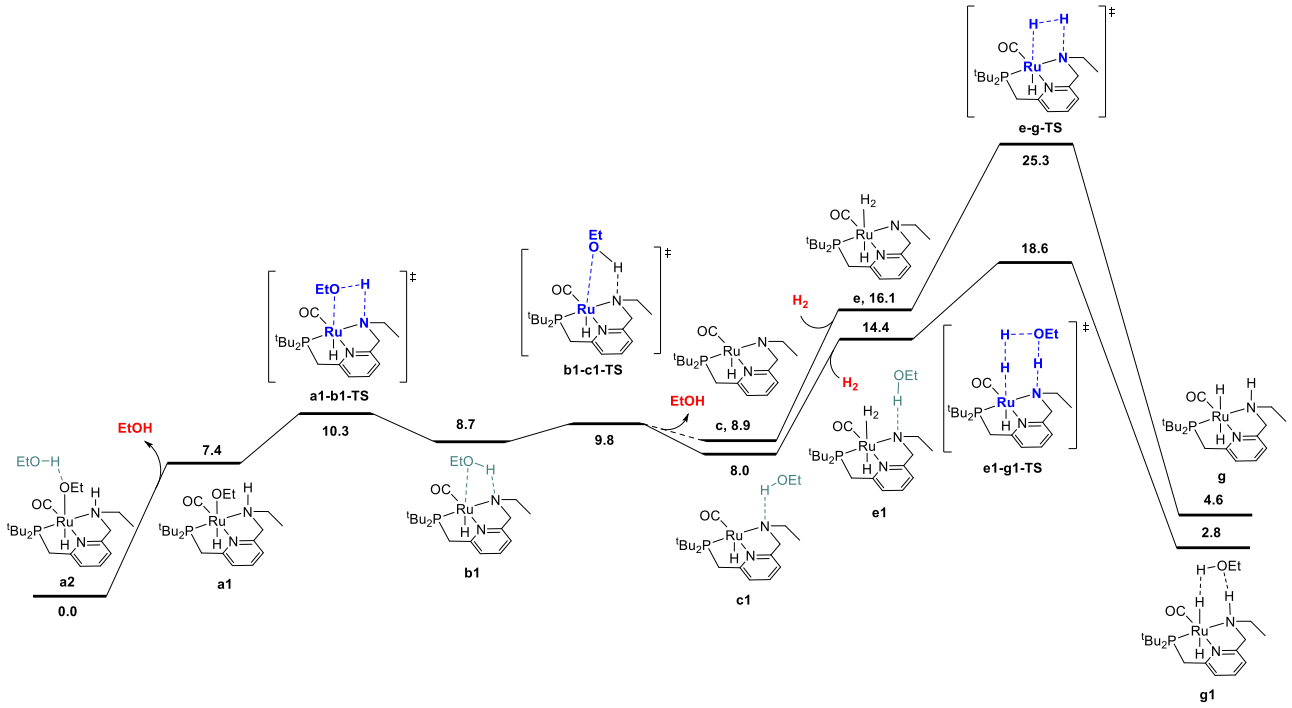

Figure S3. Alternative pathways for N-H-mediated hydrogen activation from the resting state **a2**, involving one or zero ethanol molecules as proton shuttle. For comparison, the highest barrier for the minimum-energy pathway shown in Figure 1 in the main text is 15.0 kcal/mol, corresponding to **f2-g2-TS**.

We additionally calculated sixteen pathways for the activation of hydrogen proceeding through the CH_2 linkers, as has been commonly identified as the MEP in computational studies of the original Milstein catalyst lacking an N-H group. These are grouped into four figures below. Figure S4 shows pathways with no explicit ethanol. Figure S5 shows pathways with one explicit ethanol *not* acting as a proton shuttle. Figure S6 shows pathways with one explicit ethanol acting as a proton shuttle. Last, Figure S7 shows sequences including two explicit ethanol molecules. In each figure, activation through the four diastereotopic CH_2 linker hydrogens is shown. All energies are referenced to **a2** and the organic reactants, so direct comparisons can be made with the barriers for hydrogen activation proceeding through **f2-g2-TS**, with an overall calculated barrier of 15.0 kcal/mol.

Figure S4 shows the pathways with no included proton shuttle. All four pathways shown lack a proton shuttle, and feature barriers higher than the 15.0 kcal/mol barrier for the N-H-mediated pathway shown in Figure 1 in the main text. Here, the lowest barrier of 26.7 kcal/mol is through **eN-eq-g-eq-TS**, where a proton is transferred to the NCH_2 linker *syn* to the N-H.

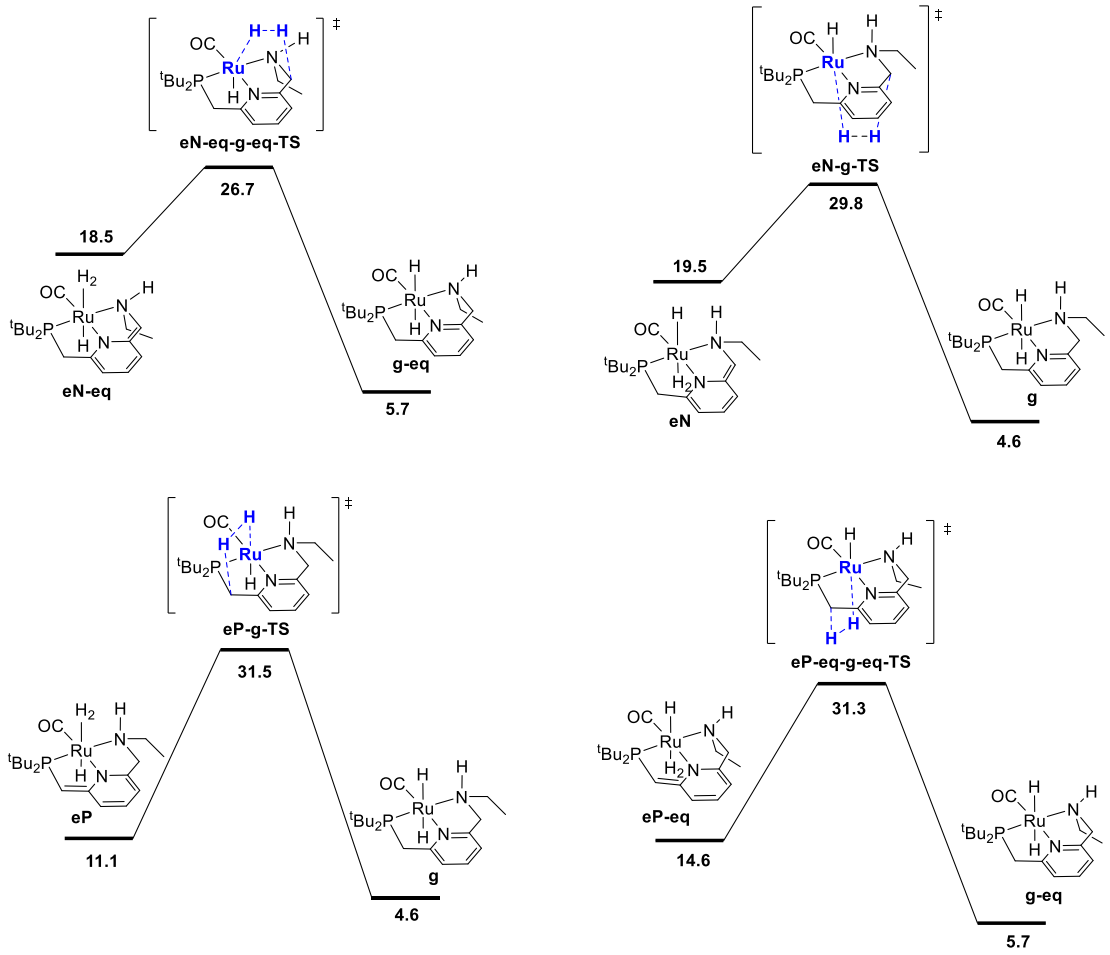

Figure S4. Alternative pathways for hydrogen activation mediated by the CH_2 linkers of the PNN-pincer ligand.

Figure S5 shows four pathways where an ethanol molecule was included with a hydrogen bond to the N-H group and potentially the ruthenium hydride, without acting as a proton shuttle. Again, all four pathways feature barriers higher than the 15.0 kcal/mol barrier for the N-H-mediated pathway shown in Figure 1 in the main text. The lowest barrier here is 31.9, indicating that an ethanol not acting as a proton shuttle does not lower the energy. This is in contrast to **a2**, which is 7.4 kcal/mol lower than **a1**, an analog lacking only a hydrogen-bonded ethanol.

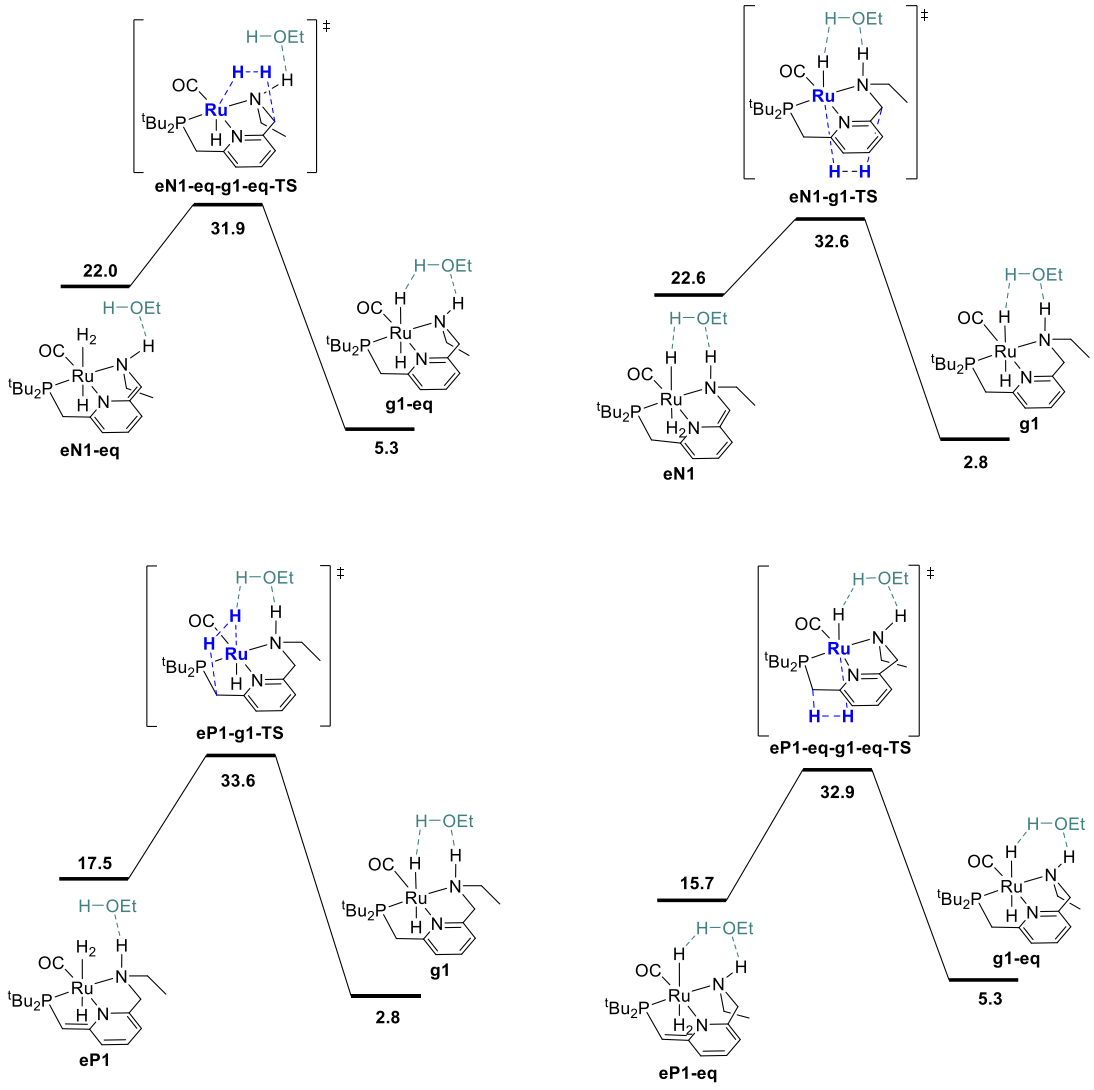

Figure S5. Alternative pathways for hydrogen activation mediated by the CH_2 linkers of the PNN-pincer ligand, including one ethanol molecule which *does not* act as a proton shuttle.

Figure S6 shows four pathways for hydrogen activation including one ethanol molecule as proton shuttle. Again, all four pathways have barriers higher than the 15.0 kcal/mol barrier in the MEP. Slightly lower barriers are found for activation of the PCH_2 linkers compared to those without a proton shuttle, but none are lower than the pathway above in Figure S4 proceeding through **eN-eq-g-eq-TS**.

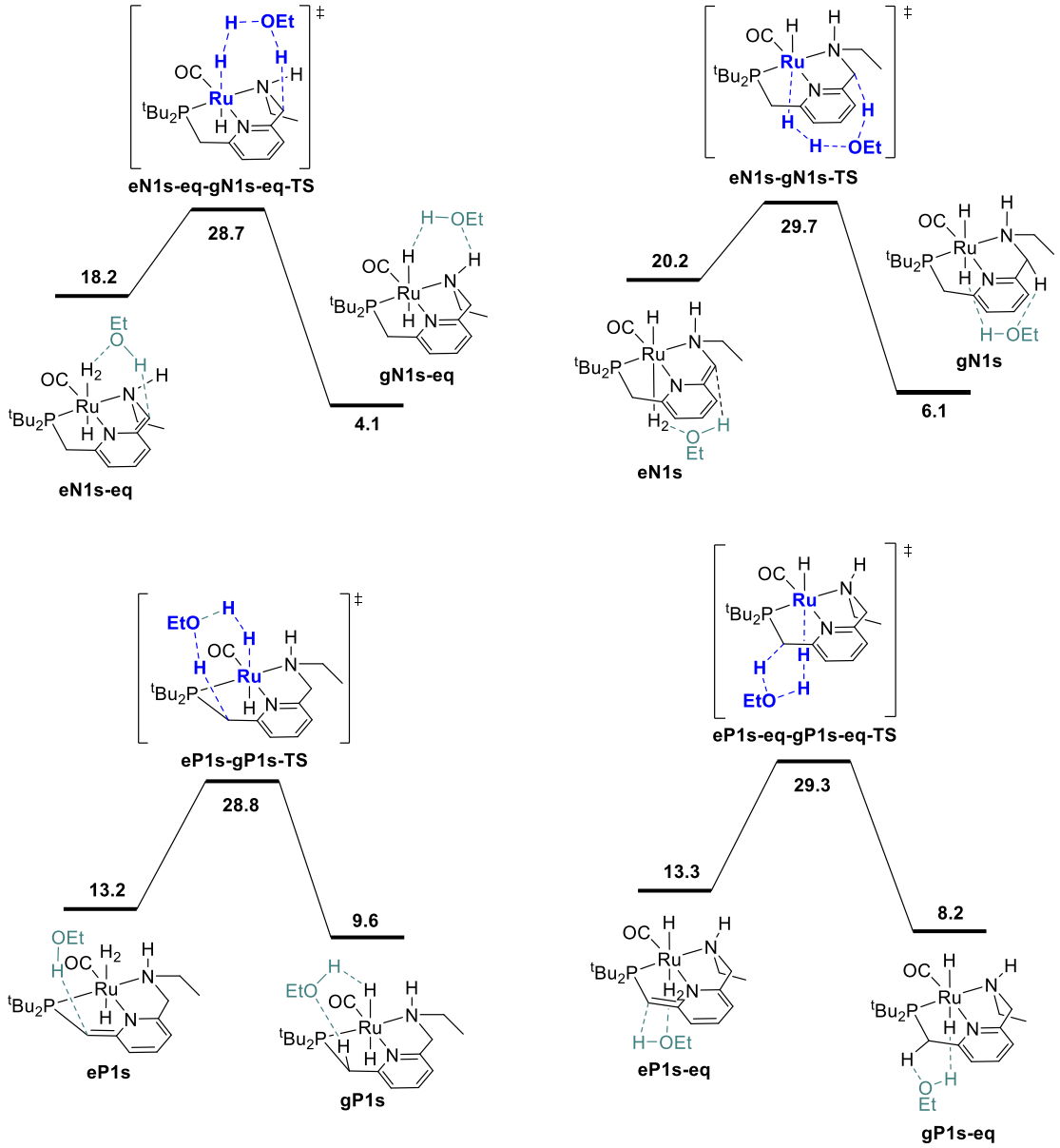

Figure S6. Alternative pathways for hydrogen activation mediated by the CH_2 linkers of the PNN-pincer ligand, including one ethanol molecule which acts as a proton shuttle.

Figure S7 shows four pathways including two ethanol molecules. In three of these pathways (top and bottom-right), one ethanol acts as a proton shuttle and the other interacts through hydrogen bonding without acting as a shuttle. In these cases, the barriers are changed minimally. All four pathways feature barriers higher than the 15.0 kcal/mol barrier for the N-H-mediated pathway shown in Figure 1 in the main text. Interestingly, hydrogen activation initiating from **eP2** (bottom-left), dearomatized by deprotonation of the PCH_2 linker, proceeds in a stepwise manner through ion-pair intermediate **fP2**, and in this way is analogous to the N-H-mediated proton-brigade mechanism in Figure 1 of the main text: the H_2 activation sequence **fP2** to **fP2-gP2-TS** to **gP2** represents a similar, higher-barrier conformation to that represented by **f2** to **f2-g2-TS** to **g2**. Since **f2** (or **fP2**) can be generated from the hydrido-alkoxide resting state **a2** as shown in Figure 1, the higher energy transition state **eP2-fP2-TS** is not on the MEP.

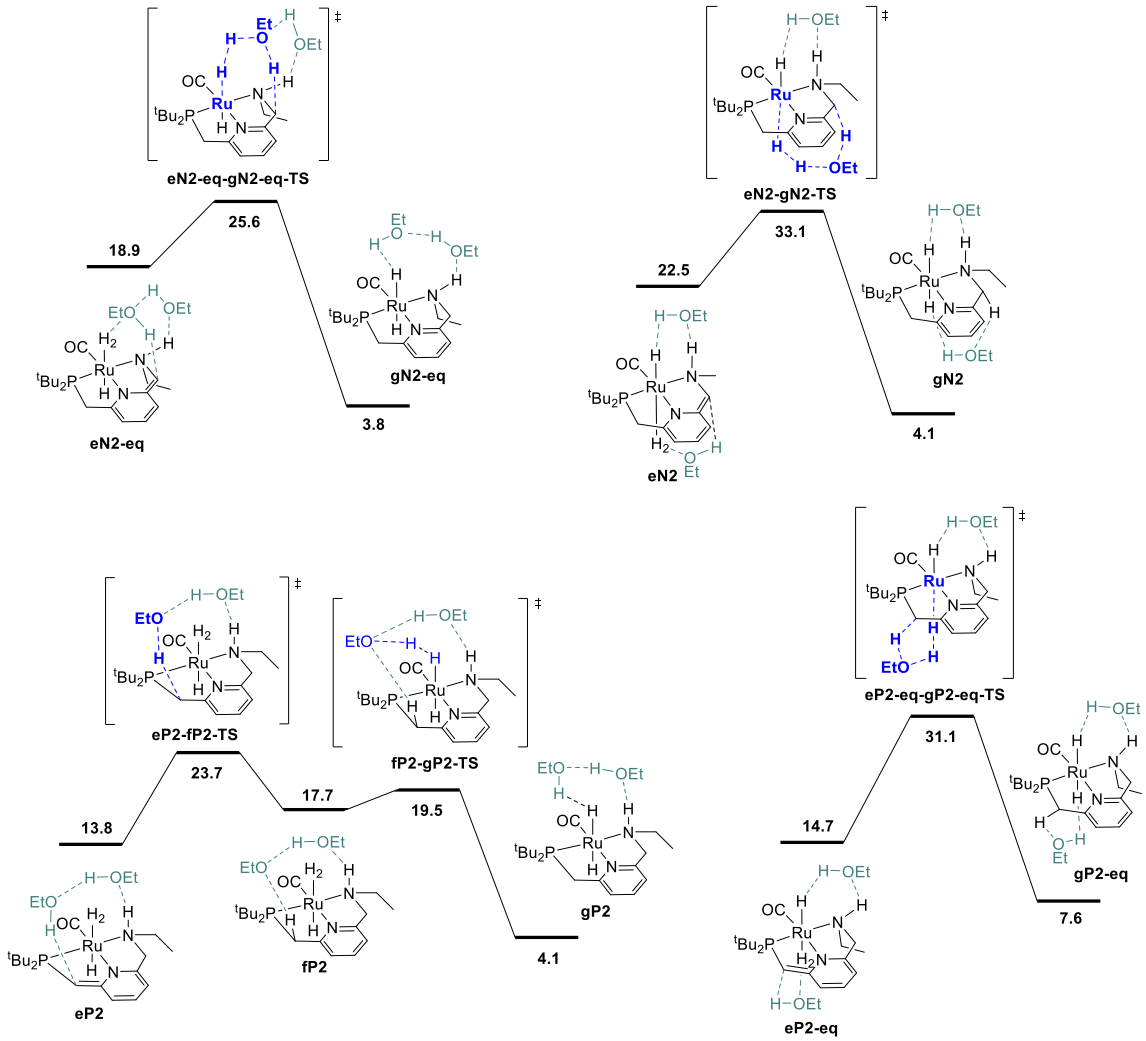

Figure S7. Alternative pathways for hydrogen activation mediated by the CH_2 linkers of the PNN-pincer ligand, including two ethanol molecules, one of which acts as a proton shuttle.

Alternative Pathways for Ester Hydrogenolysis. In addition to the MEP for ester hydrogenolysis described in Figure 2 in the main text, we identified a different pathway for C-O cleavage with a nearly identical overall barrier of 18.1 kcal/mol, which directly places the newly formed ethoxide rather than the aldehyde on ruthenium (Figure S8). Similar to the transformation identified by Hasanayn and termed a hydride-alkoxide metathesis,[13] the hemiacetal σ-complex **j** rotates through **j-o-TS** to place the ethoxy oxygen on Ru in **o**. Then, proton transfer from O to N gives **p**, and transfer of the ethoxy group from carbon to ruthenium through **p-q-TS** gives the ethoxide complex **q**, where the intermediate aldehyde is loosely associated with the N-H through a hydrogen bond. Replacement of the aldehyde with a hydrogen-bonded ethanol molecule regenerates **a2**, completing the first hydrogenation cycle. As the overall barrier of 18.1 kcal/mol for this pathway is nearly identical to the overall barrier of 17.4 kcal/mol for the pathway shown in Figure 2, our results do not unambiguously identify one pathway as preferred over the other, and it is possible that both channels operate in parallel. As an identical rate law would be predicted for either pathway, the kinetic data do not distinguish between these pathways.

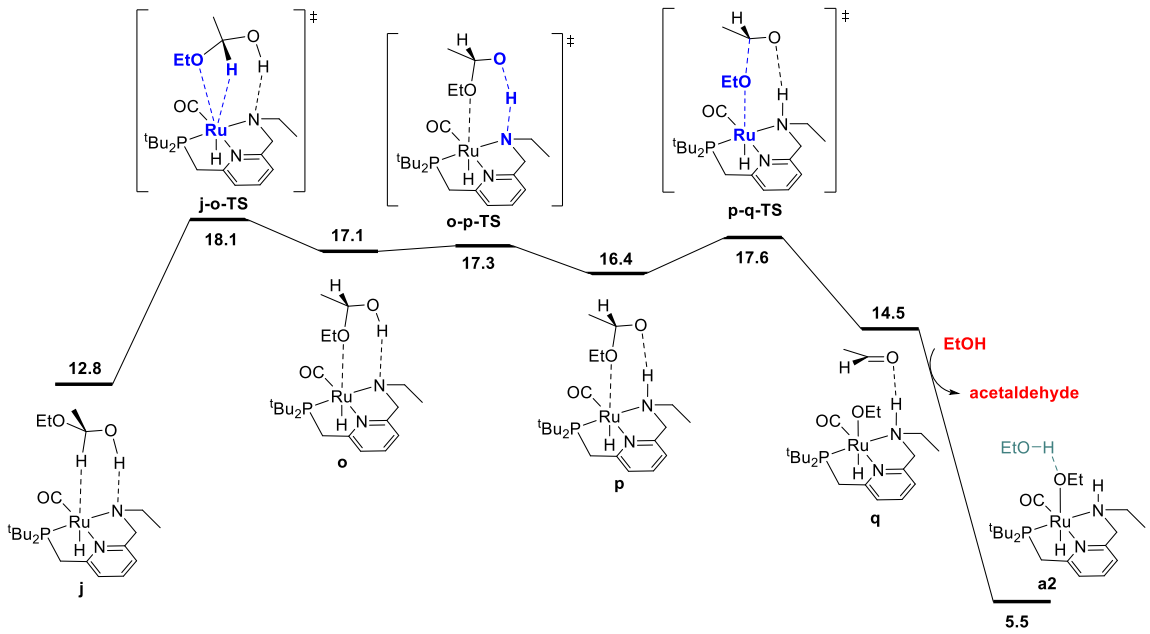

Figure S8. Alternative pathway for the conversion of hemiacetal complex **j** into hydrido-ethoxide **a2** with release of acetaldehyde, following a hydride-ethoxide metathesis pathway as proposed by Hasanayn.

In Hasanayn's pathway for hydride-alkoxide metathesis, the ligand C-H or N-H remains protonated throughout ester hydrogenolysis,[13] although the N-H is temporarily deprotonated in both of our identified mechanisms (Figure 1 and S8). We examined a direct pathway for the conversion of the hemiacetaloxide intermediate **i** to **p** through a metathesis mechanism where the N-H remains protonated, and find a slightly higher barrier of 21.4 kcal/mol (Figure S9), as compared to the 18.1 kcal/mol barrier for the pathway in Figure S8 involving the neutral hemiacetal and a deprotonated nitrogen.

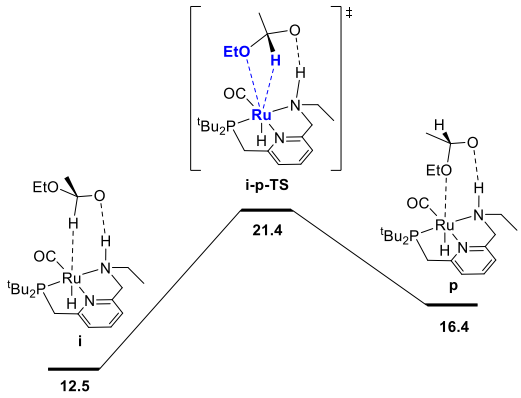

Figure S9. Alternative pathway for the conversion of C-H σ-complex **i** into O-complex **p**, following a metathesis pathway analogous to that shown in Figure 5 without prior deprotonation of nitrogen.

In addition to the pathways for ester hydrogenolysis described above, we explored diastereomeric pathways where ethyl acetate approaches ruthenium from the opposite face, pathways including an explicit ethanol molecule, and sequences where the N-H bond remains intact rather than being temporarily deprotonated. Figure S10 shows a pathway diastereomeric to the one shown in Figure 2 in the main text, which features a slightly higher overall barrier of 19.3 kcal/mol, compared with 17.4 kcal/mol in Figure 2.

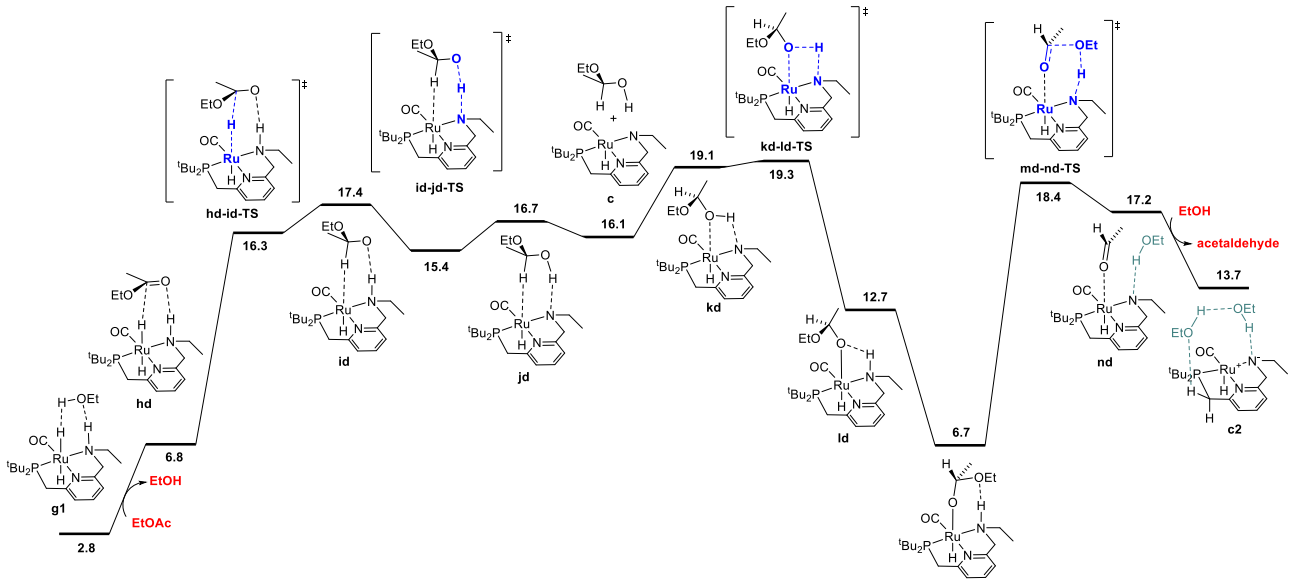

Figure S10. Alternate (diastereomeric) pathway for the hydrogenolysis of ethyl acetate along with conversion of dihydride **g1** to unsaturated intermediate **c2**.

Figure S11 shows the effect of including an explicit ethanol on the C-O bond cleavage step. Adding an ethanol molecule gives nearly the same energy barrier, which is in contrast to the strong stabilization an added ethanol molecule imparts on the resting state **a2**. Including the pathway through **m1-n1-TS** in our kinetic model was necessary to obtain a good global fit to the data.

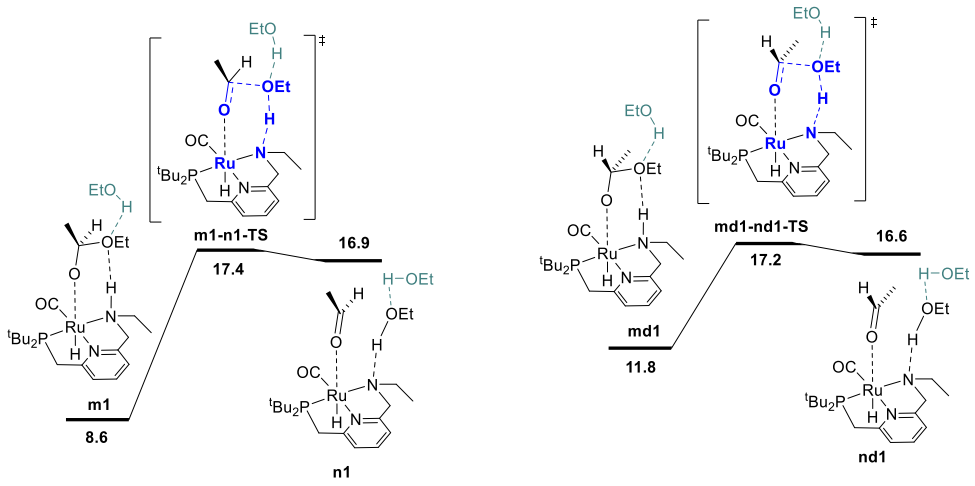

Figure S11. Alternate pathways for C-O cleavage in the hydrogenolysis of ethyl acetate, analogous to Figure XX in the main text (left) and Figure SXX in the SI (right), but featuring an explicit ethanol molecule. The analogous pathways without the added ethanol molecule have barriers of 17.4 and 18.4 kcal/mol, respectively.

Figure S12 shows a pathway diastereomeric to the Hasanayn-type pathway shown in Figure S8 above, where the alkoxide oxygen coordinates to ruthenium during C-O cleavage. The pathway in Figure S8 features a highest barrier of 18.1 kcal/mol corresponding to **j-o-TS**, as compared to the 21.1 kcal/mol barrier corresponding to **pd-qd-TS** in this scheme.

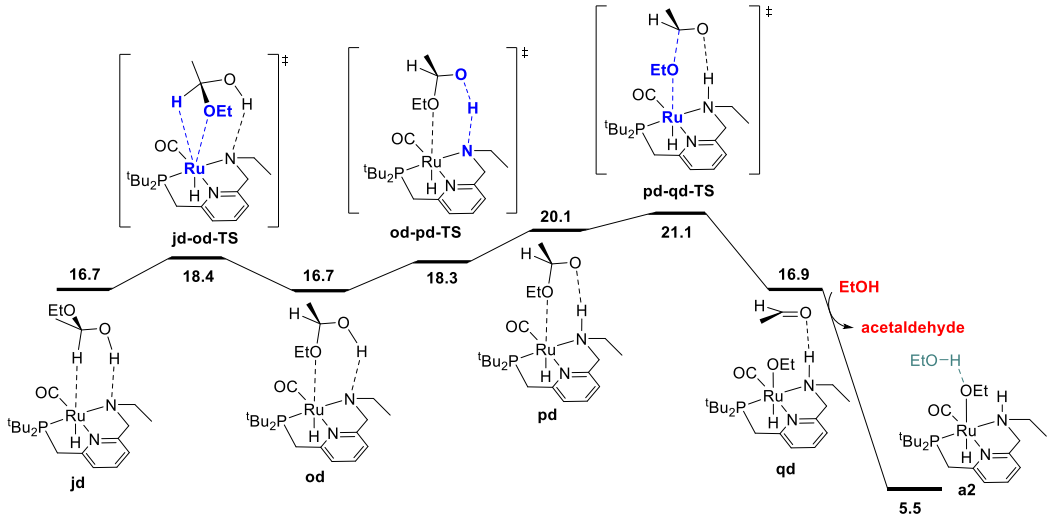

Figure S12. Alternate (diastereomeric) pathway for ester hydrogenolysis, diastereomeric to hydride-ethoxide metathesis pathway shown in Figure 5 of the main text.

Figure S13 shows a sequence diastereomeric to the pathway shown in Figure S9, where the N-H bond remains intact. The pathway in Figure S9 features a barrier of 21.4 kcal/mol corresponding to **i-p-TS**, as compared to the 21.2 kcal/mol barrier shown here. (Note that lower-barrier paths where the N-H bond is temporarily cleaved are available in both cases.)

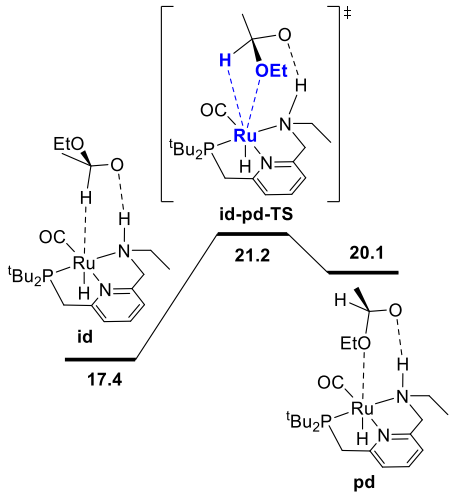

Figure S13. Alternate hydride-ethoxide metathesis pathway for ester hydrogenolysis where the N-H bond remains intact.

Figure S14 shows the minimal effect of including an explicit ethanol molecule on the Hasanayn-type transition states in Figure S9 (left) and Figure S13 (right), but featuring an explicit ethanol molecule. The analogous pathways without the added ethanol molecule have barriers of 21.4 **(i-p-TS**) and 21.2 kcal/mol (**id-pd-TS**), respectively.

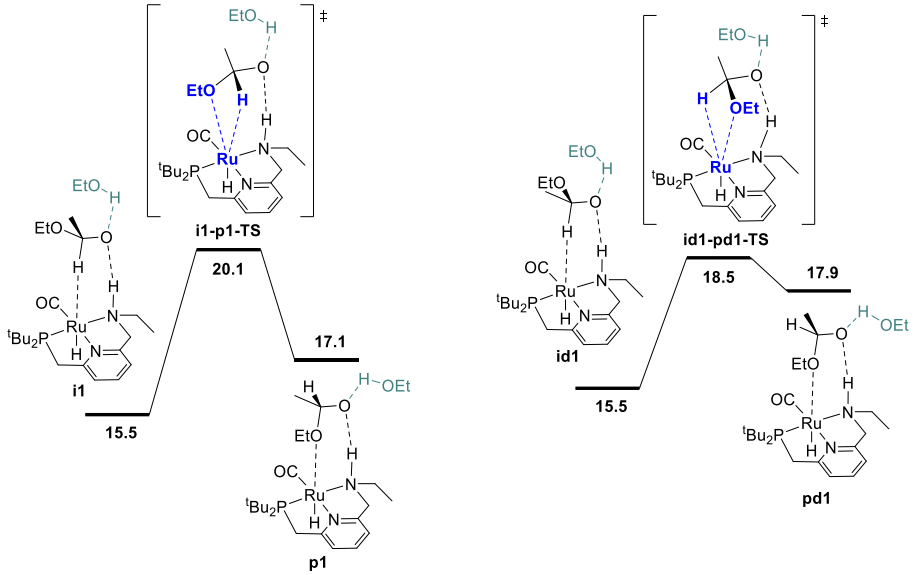

Figure S14. Alternate hydride-ethoxide metathesis pathway for ester hydrogenolysis, with explicit ethanol.

Hemiacetal Decomposition Without Ruthenium. Figure S15 shows an ethanol-catalyzed pathway for the decomposition of the hemiacetal into ethanol and aldehyde. This barrier of 36.4 kcal/mol here is much higher than the overall barrier for the ruthenium-catalyzed minimum-energy pathway of 17.4 kcal/mol shown in Figure XX in the main text.

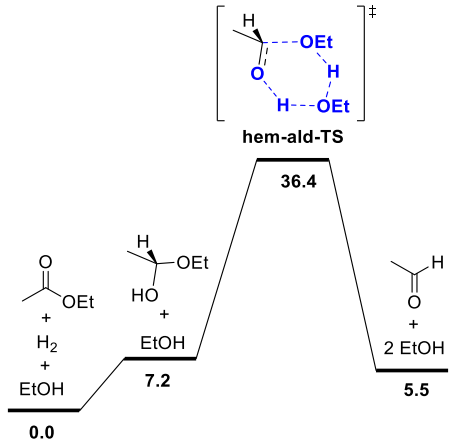

Figure S15. Alternate, ethanol-catalyzed pathway for decomposition of the hemiacetal.

Aldehyde Disproportionation. Figure S16 shows a mechanism for aldehyde disproportionation constructed using the reverse of our ester-hydrogenolysis sequence (Figure 2) followed by our aldehyde hydrogenation sequence (Figure 3). Before first binding aldehyde to form intermediate **n**, the resting state **a2** must release ethanol as in Figure 1, proceeding through **b2-c2-TS**. The entire energetic span for aldehyde disproportionation of 12.9 kcal/mol is within the pathway to eliminate ethanol from the resting-state alkoxide species, from the TDI **a2** to the TDTS **b2-c2-TS**.

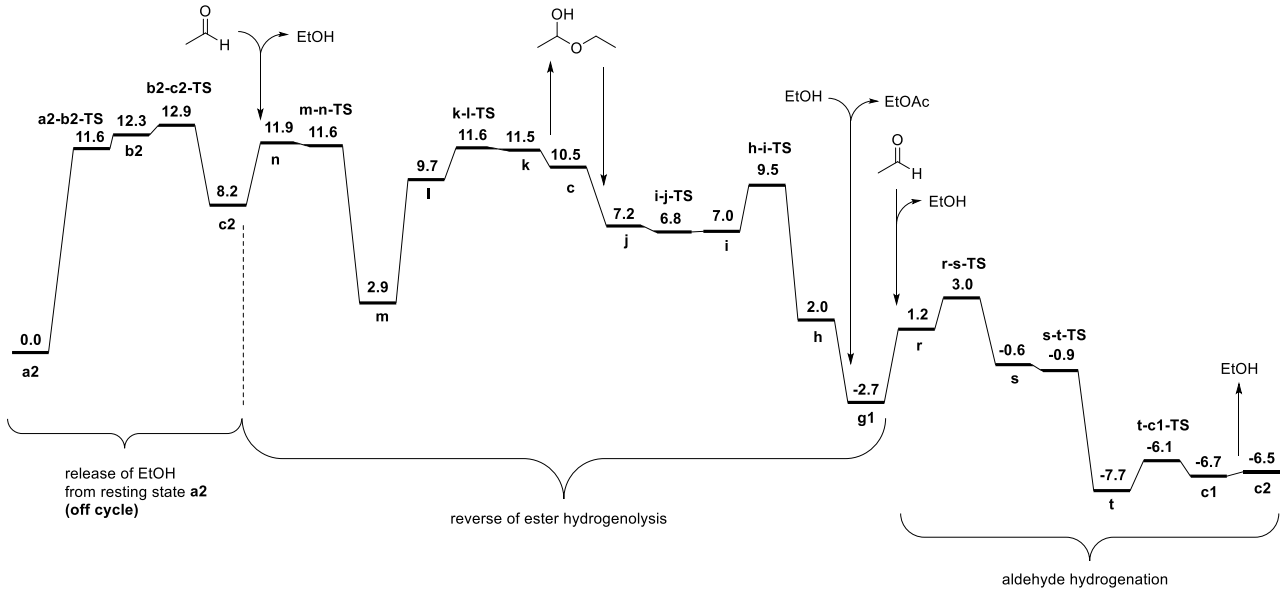

Figure S16. Reorganization of the ester hydrogenolysis and aldehyde hydrogenation pathways to give a pathway for the ruthenium-catalyzed disproportion of acetaldehyde to ethyl acetate. Free energies in kcal/mol are calculated relative to the standard state of **a2** with free acetaldehyde at 1.0 M.

Energies Calculated by DFT. Table S1 below shows the energies calculated by DFT for all structures reported in this paper. The column **E(M06/BS2)** represents the solvent-corrected electronic energy in hartrees, calculated with the M06 functional, using the LANL08(f) basis set for ruthenium and 6-311+G(2d,2p) for all other atoms. The column **G(corr)** represents the correction to the Gibbs free energy calculated at 298.15 K after geometry optimization (in solvent) using the B3LYP functional with Grimme's D3 dispersion correction,[3] with the LANL08(f) basis set for ruthenium and 6-311G(d,p) for all other atoms. The column **SS G (kcal)** represents the Gibbs free energy for each isolated species at 298.15 K in kcal/mol, including the addition of 1.89 kcal/mol for each molecule to convert to a 1 M standard state. The column **Mass Balance** lists the small molecules included in the total free energy for the calculation of reaction pathways. The column **G(total, kcal)** is the sum of free energies of the ruthenium complex and any small molecules included for mass balance. The column **G(rel)** is the total free energy referenced against **a2** with the organic reactants ethyl acetate and hydrogen. For the aldehyde disproportionation pathway at the very bottom, the reference point is instead **a2** with two molecules of acetaldehyde.

Table S1. Energies calculated by DFT

Small Molecules	E(M06/BS2)	G(corr)	SS G (kcal)
EtOH	-154.9944234	0.054528	-97224.36228
H_2	-1.170574505	-0.00144	-733.5602056
ald	-153.7866254	0.030351	-96481.6289
EtOAc	-307.6180028	0.085053	-192977.9496
hem	-308.7996752	0.109197	-193704.3096
hem-ald-TS	-463.7574784	0.17662	-290899.4906

Possible Resting States	E(M06/BS2)	G(corr)	SS G (kcal)	Mass Balance	G(total, kcal)	G(rel)
g	-1325.427975	0.429447	-831447.2396	2 EtOH	-1025895.964	4.60
g1	-1480.439681	0.501416	-928673.3924	EtOH	-1025897.755	2.81
g2	-1635.450735	0.57702	-1025896.855	none	-1025896.855	3.71
c	-1324.229866	0.407143	-830709.4103	2 EtOH + H_2	-1025891.695	8.87
c1	-1479.241268	0.480226	-927934.6738	EtOH + H_2	-1025892.596	7.97
c2	-1634.253208	0.555692	-1025158.779	H_2	-1025892.339	8.22
a1	-1479.247661	0.485729	-927935.2324	EtOH + H_2	-1025893.155	7.41
a2	-1634.271387	0.560768	-1025167.001	H_2	-1025900.561	0.00

H_2 activation	E(M06/BS2)	G(corr)	SS G (kcal)	Mass Balance	G(total, kcal)	G(rel)
a2	-1634.271387	0.560768	-1025167.001	EtOAc + 2 H_2	-1219612.071	0.00
a2-d2-TS	-1634.245453	0.557241	-1025152.941	EtOAc + 2 H_2	-1219598.011	14.06
a2-b2-TS	-1634.251546	0.559387	-1025155.417	EtOAc + 2 H_2	-1219600.487	11.58
b2	-1634.252399	0.561319	-1025154.74	EtOAc + 2 H_2	-1219599.81	12.26
b2-c2-TS	-1634.249694	0.559688	-1025154.067	EtOAc + 2 H_2	-1219599.136	12.93
c2	-1634.253208	0.555692	-1025158.779	EtOAc + 2 H_2	-1219603.849	8.22
c2-d2-TS	-1634.246417	0.552769	-1025156.352	EtOAc + 2 H_2	-1219601.422	10.65
d2	-1634.246642	0.555493	-1025154.784	EtOAc + 2 H_2	-1219599.854	12.22
e2	-1635.433256	0.572368	-1025888.806	EtOAc + H_2	-1219600.316	11.76
e2-f2-TS	-1635.429859	0.574526	-1025885.32	EtOAc + H_2	-1219596.83	15.24

f2	-1635.429337	0.572485	-1025886.273	EtOAc + H_2	-1219597.783	14.29
f2-g2-TS	-1635.426899	0.571121	-1025885.6	EtOAc + H_2	-1219597.109	14.96
g2	-1635.450735	0.57702	-1025896.855	EtOAc + H_2	-1219608.365	3.71
g1	-1480.439681	0.501416	-928673.3924	EtOAc + H_2 + EtOH	-1219609.264	2.81
Ester hydrogenolysis						
h	-1633.061133	0.537315	-1024422.273	H_2 + 2 EtOH	-1219604.557	7.51
h-i-TS	-1633.048115	0.536261	-1024414.765	H_2 + 2 EtOH	-1219597.05	15.02
i	-1633.054005	0.540469	-1024415.82	H_2 + 2 EtOH	-1219598.105	13.97
i-j-TS	-1633.05248	0.536368	-1024417.437	H_2 + 2 EtOH	-1219599.722	12.35
j	-1633.054084	0.538611	-1024417.036	H_2 + 2 EtOH	-1219599.321	12.75
c + hem	-1324.229866	0.407143	-830709.4103	H_2 + 2 EtOH + hem	-1219596.005	16.07
k	-1633.046728	0.537995	-1024412.806	H_2 + 2 EtOH	-1219595.091	16.98
k-l-TS	-1633.043634	0.535188	-1024412.626	H_2 + 2 EtOH	-1219594.911	17.16
l	-1633.052154	0.540682	-1024414.525	H_2 + 2 EtOH	-1219596.81	15.26
m	-1633.066357	0.543966	-1024421.377	H_2 + 2 EtOH	-1219603.662	8.41
m-n-TS	-1633.04206	0.533598	-1024412.636	H_2 + 2 EtOH	-1219594.921	17.15
n	-1633.04463	0.536518	-1024412.417	H_2 + 2 EtOH	-1219594.701	17.37
i-p-TS	-1633.039899	0.538255	-1024408.358	H_2 + 2 EtOH	-1219590.643	21.43
p	-1633.050379	0.5408	-1024413.337	H_2 + 2 EtOH	-1219595.622	16.45
p-q-TS	-1633.048832	0.541062	-1024412.202	H_2 + 2 EtOH	-1219594.487	17.58
q	-1633.049947	0.537292	-1024415.267	H_2 + 2 EtOH	-1219597.552	14.52
j-o-TS	-1633.046757	0.539884	-1024411.639	H_2 + 2 EtOH	-1219593.924	18.15
o	-1633.049689	0.541138	-1024412.692	H_2 + 2 EtOH	-1219594.977	17.09
o-p-TS	-1633.046702	0.538431	-1024412.517	H_2 + 2 EtOH	-1219594.801	17.27
Aldehyde hydrogenation						
r	-1479.228019	0.479652	-927926.72	3 EtOH	-1219599.807	12.26
r-s-TS	-1479.225247	0.479761	-927924.9124	3 EtOH	-1219597.999	14.07
s	-1479.236721	0.485431	-927928.5543	3 EtOH	-1219601.641	10.43
s-t-TS	-1479.236918	0.485094	-927928.8891	3 EtOH	-1219601.976	10.10
t	-1479.2445	0.481976	-927935.6038	3 EtOH	-1219608.691	3.38
t-c1-TS	-1479.242274	0.482155	-927934.0945	3 EtOH	-1219607.181	4.89
c1 (ref. to products)	-1479.241268	0.480226	-927934.6738	3 EtOH	-1219607.761	4.31
Supporting Information: Hydrogen Activation Alternatives						
a1	-1479.247661	0.485729	-927935.2324	EtOAc + 2 H_2 + EtOH	-1219604.665	7.41
a1-b1-TS	-1479.238966	0.481653	-927932.3335	EtOAc + 2 H_2 + EtOH	-1219601.766	10.31
b1	-1479.242412	0.482546	-927933.9355	EtOAc + 2 H_2 + EtOH	-1219603.368	8.70
b1-c1-TS	-1479.241071	0.482954	-927932.8382	EtOAc + 2 H_2 + EtOH	-1219602.27	9.80
c1	-1479.241268	0.480226	-927934.6738	EtOAc + 2 H_2 + EtOH	-1219604.106	7.97
e1	-1480.418236	0.498468	-928661.7852	EtOAc + H_2 + EtOH	-1219597.657	14.41
e1-g1-TS	-1480.408997	0.495962	-928657.5601	EtOAc + H_2 + EtOH	-1219593.432	18.64
g1	-1480.439681	0.501416	-928673.3924	EtOAc + H_2 + EtOH	-1219609.264	2.81
g	-1325.427975	0.429447	-831447.2396	EtOAc + H_2 + 2 EtOH	-1219607.474	4.60
c	-1324.229866	0.407143	-830709.4103	EtOAc + 2 H_2 + 2 EtOH	-1219603.205	8.87
e	-1325.403176	0.422917	-831435.7756	EtOAc + H_2 + 2 EtOH	-1219596.01	16.06

e-g-TS	-1325.386861	0.421264	-831426.5749	EtOAc + H_2 + 2 EtOH	-1219586.809	25.26
eN-eq	-1325.401593	0.425259	-831433.3122	EtOAc + H_2 + 2 EtOH	-1219593.547	18.52
eN-eq-g-eq-TS	-1325.385909	0.422631	-831425.1196	EtOAc + H_2 + 2 EtOH	-1219585.354	26.72
g-eq	-1325.426619	0.429807	-831446.1628	EtOAc + H_2 + 2 EtOH	-1219606.397	5.67
eN	-1325.401468	0.426626	-831432.3761	EtOAc + H_2 + 2 EtOH	-1219592.61	19.46
eN-g-TS	-1325.384359	0.425944	-831422.0682	EtOAc + H_2 + 2 EtOH	-1219582.302	29.77
eP	-1325.413341	0.425112	-831440.7768	EtOAc + H_2 + 2 EtOH	-1219601.011	11.06
eP-g-TS	-1325.378713	0.423063	-831420.3327	EtOAc + H_2 + 2 EtOH	-1219580.567	31.50
eP-eq	-1325.410892	0.428328	-831437.2217	EtOAc + H_2 + 2 EtOH	-1219597.456	14.62
eP-eq-g-eq-TS	-1325.37852	0.422606	-831420.4986	EtOAc + H_2 + 2 EtOH	-1219580.733	31.34
eN1-eq	-1480.407075	0.499448	-928654.1664	EtOAc + H_2 + EtOH	-1219590.038	22.03
eN1-eq-g1-eq-TS	-1480.390996	0.499057	-928644.3225	EtOAc + H_2 + EtOH	-1219580.195	31.88
eN1	-1480.406921	0.500198	-928653.5994	EtOAc + H_2 + EtOH	-1219589.471	22.60
eN1-g1-TS	-1480.391712	0.500884	-928643.6248	EtOAc + H_2 + EtOH	-1219579.497	32.57
eP1	-1480.417936	0.503121	-928658.6773	EtOAc + H_2 + EtOH	-1219594.549	17.52
eP1-g1-TS	-1480.388743	0.499541	-928642.6047	EtOAc + H_2 + EtOH	-1219578.477	33.59
eP1-eq	-1480.417263	0.499564	-928660.4872	EtOAc + H_2 + EtOH	-1219596.359	15.71
eP1-eq-g1-eq-TS	-1480.385581	0.49521	-928643.3384	EtOAc + H_2 + EtOH	-1219579.21	32.86
g1-eq	-1480.436478	0.502153	-928670.92	EtOAc + H_2 + EtOH	-1219606.792	5.28
eN1s-eq	-1480.411309	0.497594	-928657.9866	EtOAc + H_2 + EtOH	-1219593.859	18.21
eN1s-eq-gN1s-eq-TS	-1480.392336	0.495334	-928647.4995	EtOAc + H_2 + EtOH	-1219583.371	28.70
gN1s-eq	-1480.436428	0.500209	-928672.1083	EtOAc + H_2 + EtOH	-1219607.98	4.09
eN1s	-1480.409885	0.499306	-928656.0189	EtOAc + H_2 + EtOH	-1219591.891	20.18
eN1s-gN1s-TS	-1480.389452	0.494036	-928646.504	EtOAc + H_2 + EtOH	-1219582.376	29.70
gN1s	-1480.434742	0.501669	-928670.1339	EtOAc + H_2 + EtOH	-1219606.006	6.07
eP1s	-1480.420105	0.498384	-928663.0107	EtOAc + H_2 + EtOH	-1219598.883	13.19
eP1s-gP1s-TS	-1480.392609	0.495809	-928647.3723	EtOAc + H_2 + EtOH	-1219583.244	28.83
gP1s	-1480.436349	0.508832	-928666.648	EtOAc + H_2 + EtOH	-1219602.52	9.55
eP1s-eq	-1480.420437	0.498966	-928662.8537	EtOAc + H_2 + EtOH	-1219598.726	13.35
eP1s-eq-gP1s-eq-TS	-1480.393161	0.497062	-928646.9329	EtOAc + H_2 + EtOH	-1219582.805	29.27
gP1s-eq	-1480.434031	0.504347	-928668.0074	EtOAc + H_2 + EtOH	-1219603.879	8.19
eN2-eq	-1635.421468	0.571918	-1025881.691	EtOAc + H_2	-1219593.201	18.87
eN2-eq-gN2-eq-TS	-1635.408675	0.569864	-1025874.953	EtOAc + H_2	-1219586.462	25.61
gN2-eq	-1635.450583	0.577035	-1025896.75	EtOAc + H_2	-1219608.26	3.81
eN2	-1635.416572	0.572757	-1025878.092	EtOAc + H_2	-1219589.602	22.47
eN2-gN2-TS	-1635.39598	0.56903	-1025867.51	EtOAc + H_2	-1219579.019	33.05
gN2	-1635.446515	0.573456	-1025896.443	EtOAc + H_2	-1219607.953	4.12
eP2	-1635.432957	0.575336	-1025886.756	EtOAc + H_2	-1219598.266	13.81
eP2-fP2-TS	-1635.413985	0.572138	-1025876.857	EtOAc + H_2	-1219588.367	23.70
fP2	-1635.423748	0.572304	-1025882.88	EtOAc + H_2	-1219594.39	17.68
eP2-eq	-1635.428367	0.572094	-1025885.91	EtOAc + H_2	-1219597.42	14.65
eP2-eq-gP2-eq-TS	-1635.400648	0.570549	-1025869.485	EtOAc + H_2	-1219580.995	31.08
gP2-eq	-1635.445083	0.577587	-1025892.953	EtOAc + H_2	-1219604.463	7.61
fP2-gP2-TS	-1635.423088	0.574614	-1025881.016	EtOAc + H_2	-1219592.526	19.55
gP2	-1635.449472	0.576336	-1025896.492	EtOAc + H_2	-1219608.001	4.07

Supporting Information: Ester Hydrogenolysis Alternatives

hd	-1633.059341	0.53444	-1024422.952	H_2 + 2 EtOH	-1219605.237	6.83
hd-id-TS	-1633.047684	0.53779	-1024413.535	H_2 + 2 EtOH	-1219595.82	16.25
id	-1633.050005	0.54195	-1024412.381	H_2 + 2 EtOH	-1219594.666	17.41
id-jd-TS	-1633.047904	0.536636	-1024414.397	H_2 + 2 EtOH	-1219596.682	15.39
jd	-1633.051062	0.541929	-1024413.058	H_2 + 2 EtOH	-1219595.342	16.73
kd	-1633.045273	0.539941	-1024410.672	H_2 + 2 EtOH	-1219592.957	19.11
kd-ld-TS	-1633.042366	0.537359	-1024410.468	H_2 + 2 EtOH	-1219592.753	19.32
ld	-1633.05901	0.543433	-1024417.101	H_2 + 2 EtOH	-1219599.386	12.69
md	-1633.068489	0.543406	-1024423.066	H_2 + 2 EtOH	-1219605.351	6.72
md-nd-TS	-1633.041612	0.53516	-1024411.375	H_2 + 2 EtOH	-1219593.66	18.41
nd	-1633.044655	0.536246	-1024412.603	H_2 + 2 EtOH	-1219594.888	17.18
m1	-1788.075278	0.616266	-1121645.574	H_2 + EtOH	-1219603.497	8.57
m1-n1-TS	-1788.052379	0.607426	-1121636.752	H_2 + EtOH	-1219594.675	17.40
n1	-1788.052325	0.60664	-1121637.211	H_2 + EtOH	-1219595.134	16.94
md1	-1788.07319	0.61929	-1121642.366	H_2 + EtOH	-1219600.289	11.78
md1-nd1-TS	-1788.053158	0.60785	-1121636.975	H_2 + EtOH	-1219594.898	17.17
nd1	-1788.053331	0.607043	-1121637.59	H_2 + EtOH	-1219595.512	16.56
id-pd-TS	-1633.041749	0.539808	-1024408.544	H_2 + 2 EtOH	-1219590.829	21.24
pd	-1633.046755	0.542954	-1024409.712	H_2 + 2 EtOH	-1219591.996	20.07
pd-qd-TS	-1633.045413	0.543175	-1024408.731	H_2 + 2 EtOH	-1219591.015	21.06
qd	-1633.045143	0.536279	-1024412.889	H_2 + 2 EtOH	-1219595.174	16.90
jd-od-TS	-1633.047162	0.540738	-1024411.358	H_2 + 2 EtOH	-1219593.643	18.43
od	-1633.051064	0.541913	-1024413.069	H_2 + 2 EtOH	-1219595.353	16.72
od-pd-TS	-1633.045307	0.53871	-1024411.466	H_2 + 2 EtOH	-1219593.751	18.32
i1	-1788.059912	0.61194	-1121638.647	H_2 + EtOH	-1219596.569	15.50
i1-p1-TS	-1788.054648	0.614075	-1121634.004	H_2 + EtOH	-1219591.926	20.14
p1	-1788.062046	0.616621	-1121637.048	H_2 + EtOH	-1219594.971	17.10
id1	-1788.065957	0.617941	-1121638.674	H_2 + EtOH	-1219596.597	15.47
id1-pd1-TS	-1788.058846	0.615703	-1121635.617	H_2 + EtOH	-1219593.539	18.53
pd1	-1788.063446	0.619261	-1121636.27	H_2 + EtOH	-1219594.193	17.88

Supporting Information: Aldehyde Disproportionation Pathway

a2	-1634.271387	0.560768	-1025167.001	2 ald	-1218130.259	0.00
a2-b2-TS	-1634.251546	0.559387	-1025155.417	2 ald	-1218118.675	11.58
b2	-1634.252399	0.561319	-1025154.74	2 ald	-1218117.998	12.26
b2-c2-TS	-1634.249694	0.559688	-1025154.067	2 ald	-1218117.324	12.93
c2	-1634.253208	0.555692	-1025158.779	2 ald	-1218122.036	8.22
n	-1633.04463	0.536518	-1024412.417	ald + EtOH	-1218118.408	11.85
m-n-TS	-1633.04206	0.533598	-1024412.636	ald + EtOH	-1218118.628	11.63
m	-1633.066357	0.543966	-1024421.377	ald + EtOH	-1218127.368	2.89
l	-1633.052154	0.540682	-1024414.525	ald + EtOH	-1218120.516	9.74
k-l-TS	-1633.043634	0.535188	-1024412.626	ald + EtOH	-1218118.617	11.64
k	-1633.046728	0.537995	-1024412.806	ald + EtOH	-1218118.798	11.46
c + hem	-1324.229866	0.407143	-830709.4103	ald + EtOH + hem	-1218119.711	10.55
j	-1633.054084	0.538611	-1024417.036	ald + EtOH	-1218123.027	7.23

i-j-TS	-1633.05248	0.536368	-1024417.437	ald + EtOH	-1218123.428	6.83
i	-1633.054072	0.538234	-1024417.265	ald + EtOH	-1218123.256	7.00
h-i-TS	-1633.048115	0.536261	-1024414.765	ald + EtOH	-1218120.756	9.50
h	-1633.061133	0.537315	-1024422.273	ald + EtOH	-1218128.264	2.00
g1	-1480.439681	0.501416	-928673.3924	ald + EtOAc	-1218132.971	-2.71
r	-1479.228019	0.479652	-927926.72	EtOH + EtOAc	-1218129.032	1.23
r-s-TS	-1479.225247	0.479761	-927924.9124	EtOH + EtOAc	-1218127.224	3.03
s	-1479.236721	0.485431	-927928.5543	EtOH + EtOAc	-1218130.866	-0.61
s-t-TS	-1479.236918	0.485094	-927928.8891	EtOH + EtOAc	-1218131.201	-0.94
t	-1479.2445	0.481976	-927935.6038	EtOH + EtOAc	-1218137.916	-7.66
t-c1-TS	-1479.242274	0.482155	-927934.0945	EtOH + EtOAc	-1218136.406	-6.15
c1	-1479.241268	0.480226	-927934.6738	EtOH + EtOAc	-1218136.986	-6.73
c2	-1634.253208	0.555692	-1025158.779	EtOAc	-1218136.728	-6.47

Comparison with Previously Reported Mechanisms. Because we have proposed a new mechanism for ester hydrogenation catalyzed by the activated (NHEt) form of Milstein's catalyst with an overall barrier of 17.4 kcal/mol, it is instructive to compare to previously reported pathways that used the nonactivated (NEt_2) form of Milstein's catalyst, which we have shown is not kinetically competent as a catalyst. Figure S17 shows Wang and coworkers' pathway,[14] Figure S18 shows Zhang and coworkers' pathway,[15] and Figure S19 shows Gusev's pathway.[16]

In Wang's study,[16] barriers for ADC of alcohols to esters were compared with barriers for dehydrogenative amine-alcohol coupling to give amides. Using their reported structures and energies, we have calculated the MEP for ester hydrogenation, which is the reverse of the ADC reaction (Figure S17). Raw free energies for most species (optimization at TPSSTPSS/LanL2DZ(Ru)/6-31G(d,p)/gas phase, single-point refinement at TPSSTPSS/LanL2DZ(Ru)/6-31++G(d,p)/IEFPCM,toluene, 298.15 K) were taken directly from the Supporting Information. In the Supporting Information, the raw free energy for hydrogen was omitted and the raw free energy for **TS21** of -1673.722565 appeared to be for a molecule with a different formula, so these values were back-calculated from the relative free energies given in the main manuscript. G(tot, 1 atm, hartree) is calculated by summing the appropriate small molecules for mass balance. G(tot, 1 atm, kcal/mol) is calculated using the conversion of 627.509474 kcal/mol·hartree. G(relative, kcal/mol) is calculated taking **33'** as the reference. The resting state and TDI is the dihydride species **5dih**, and the TDTS is the proton-transfer transition-state **TS16**. In this sequence, the energetic span is 38.5 kcal/mol. Wang and coworkers also discussed two schemes for correction of the free energies to better model solution-phase enthalpies, either adding 4.3 kcal/mol to each molecule as proposed by Martin, Hay, and Pratt,[17] or adding half this value based on work by Yu and Houk.[18] Applying these schemes changes the energetic span to 34.2 and 36.4 kcal/mol, respectively. As the Yu/Houk scheme involves adding 2.15 kcal/mol to each species, its effect on the overall energy surface is very similar to the standard-state correction we have applied in our calculations, which involves adding 1.89 kcal/mol to convert each species from 1 atm to 1 M.

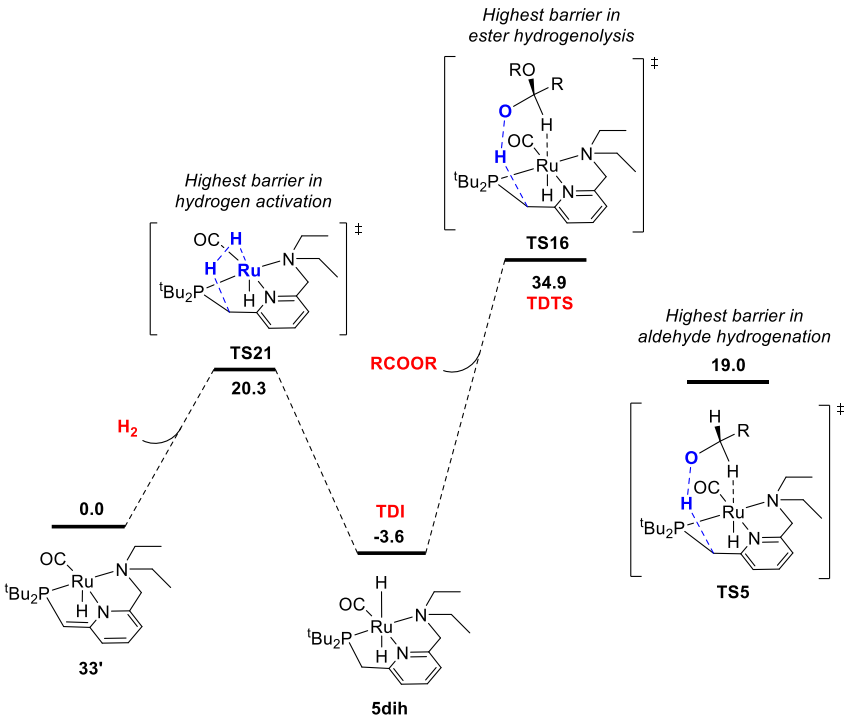

Small Molecules	G (1 atm, hartree)
alcohol	-269.525972
aldehyde	-268.336283
hydrogen	-1.17680303
ester	-536.687915

Ruthenium complexes	G (1 atm, hartree)	Mass Balance	G(tot, 1 atm, hartree)	G(1 atm, kcal/mol)	G(relative, kcal/mol)
33'	-1402.964288	2 H_2 + RCH_2OR	-1942.005809	-1218627.044	0.0
TS21	-1404.108741	H_2 + RCH_2OR	-1941.973459	-1218606.744	20.3
5dih	-1404.146828	H_2 + RCH_2OR	-1942.011546	-1218630.644	**-3.6**
TS16	-1940.773373	H_2	-1941.950176	-1218592.133	**34.9**
TS5	-1672.449581	ROH	-1941.975553	-1218608.058	19.0

Figure S17. Recalculation of the energetic span for ester hydrogenation based on Wang and coworkers' computed mechanism for the reverse ADC reaction.[14]

In Zhang's study,[15] a pathway was calculated for ester hydrogenation, and all energies given in the manuscript were already referenced against the resting state **Ru^{II}PNN** (which we have called **RuPNN^{dearom}** in our paper). As such, no adjustment of the energies was necessary to calculate the energetic span. Figure S18 shows a simplified scheme, including only the highest barriers along the hydrogen-activation and ester-hydrogenolysis pathways. The resting state and TDI is the dearomatized species **Ru^{II}PNN**, and the TDTS is the hydride-transfer transition-state **TS10**. In this sequence, the energetic span is 27.2 kcal/mol.

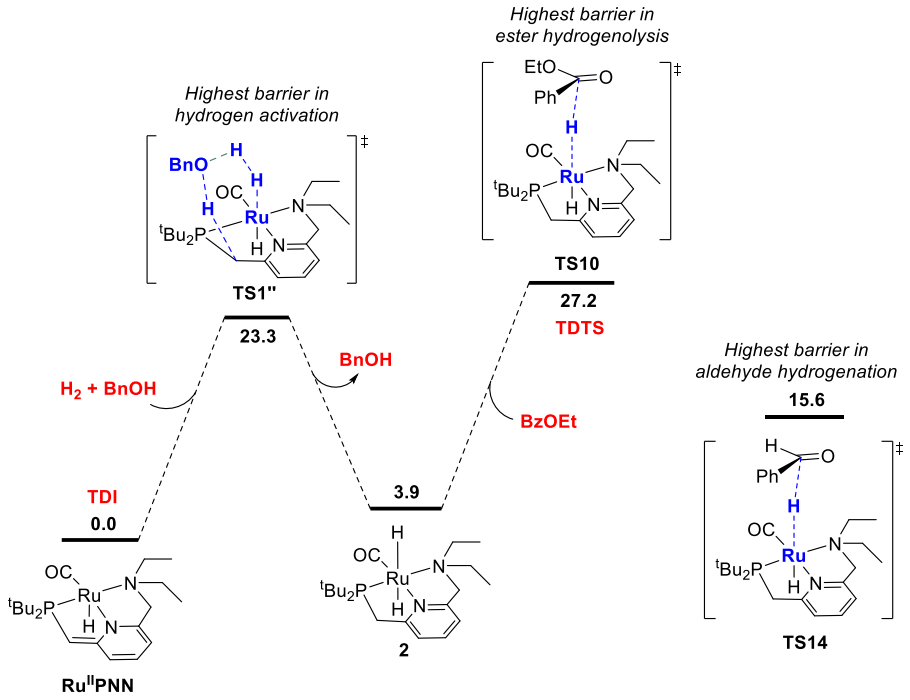

Figure S18. Simplified diagram of Zhang and coworkers' computed mechanism for ester hydrogenation.[15]

In Gusev's study,[16] a pathway for the ADC reaction was calculated. Using his reported structures and energies, we have calculated the MEP for ester hydrogenation, which is the reverse of the ADC reaction (Figure S19). Raw free energies (M06-L, SMD-toluene, Def2QXVP with def2 ECP on Ru, Def2SVPD with W06 density fitting on other atoms, 298.15 K) were taken directly from the Supporting Information. G(tot, 1 atm, hartree) is calculated by summing the appropriate small molecules for mass balance. G(tot, 1 atm, kcal/mol) is calculated by using the conversion of 627.509474 kcal/mol·hartree. G(1M, kcal/mol) is calculated by adding 1.89 kcal/mol to every molecular species except for hydrogen, to convert their standard states from 1 atm to 1 M. G(relative, kcal/mol) is calculated taking **4·EtOH** as the reference. The resting state and TDI is the ethanol-stabilized hydrido-alkoxide species **4·EtOH**, and the TDTS is the Hasanayn-type hydride-alkoxide metathesis transition-state **TS11**. In this sequence, the energetic span is 31.8 kcal/mol. If the hydrogen standard state is taken as 1M (as we have done in this paper) instead of 1 atm (as done in Gusev's work), the energetic span becomes 29.9 kcal/mol.

Small Molecules	G (1 atm, hartree)
H2	-1.168832
EtOH	-154.860791
EtOAc	-307.377125
acetaldehyde	-153.678648

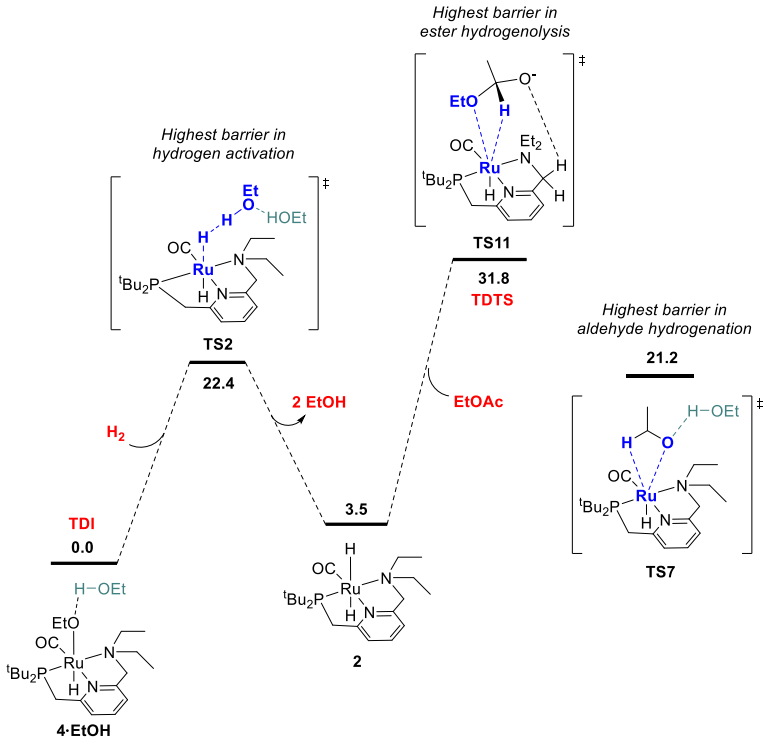

Ruthenium complexes	G (1 atm, hartree)	Mass Balance	G(tot, 1 atm, hartree)	G(tot, 1 atm, kcal/mol)	G(1M, kcal/mol)	G(relative, kcal/mol)
4·EtOH	-1712.776860	2 H_2 + EtOAc	-2022.491649	-1269132.671	-1269128.891	**0.0**
TS2	-1713.910035	H_2 + EtOAc	-2022.455992	-1269110.296	-1269106.516	22.4
2	-1404.224580	H_2 + EtOAc + 2 EtOH	-2022.492119	-1269132.966	-1269125.406	3.5
TS11	-1711.553624	H_2 + 2 EtOH	-2022.444038	-1269102.794	-1269097.124	**31.8**
TS7	-1712.739270	2 EtOH	-2022.460852	-1269113.345	-1269107.675	21.2

Figure S19. Recalculation of the energetic span for ester hydrogenation based on Gusev's computed mechanism for the reverse ADC reaction.[16]

Synthesis of RuPNN^{HEt}. RuPNN^{HEt} was previously characterized by NMR spectroscopy in solution under 10 bar H_2 in C_6D_6.[1] Here we report the isolation of **RuPNN^{HEt}** in crystalline form following a procedure analogous to that reported by Gusev for the isolation of **RuPNN^{H2}**.[16] In an argon glovebox, **RuPNN^{imine}** (316 mg, 0.450 mmol) was dissolved in 6.0 mL toluene in a 40 mL vial. Then, 30 mL pentane was added to the vial, and the dark purple solution was briefly swirled to mix. The open vial was placed in a 450 mL Parr pressure reactor, which was sealed and brought out of the glovebox. The vessel was then pressurized with hydrogen to 30 bar and allowed to sit at room temperature for three days without stirring. The pressure vessel was carefully vented, closed (with one atmosphere of hydrogen remaining), brought into the glovebox, and opened. The vial was removed and observed to contain yellow crystals and a pale purple/brown mother liquor. The crystals were collected and washed several times with pentane, then dried under vacuum for only one hour. Yield: 160 mg, 84% The product **RuPNN^{HEt}** is stable under inert atmosphere in the solid state for several days at room temperature, and is stable for months under inert atmosphere at -37 °C. However, dissolution in benzene-d_6 at room temperature resulted in rapid formation of a brown solution, and the NMR spectrum indicated decomposition. Dissolving in toluene-d_8 at -37 °C and recording NMR spectra at -30 °C allowed confirmation that this product matches the sample of **RuPNN^{HEt}**

previously characterized only in solution under hydrogen pressure.[1] X-ray crystallography confirmed that the crystalline product contains one half-equivalent of toluene per ruthenium complex, which was consistent with elemental analysis data. Anal. calcd. for $C_{18}H_{33}N_2OPRu \cdot \frac{1}{2}(C_7H_8)$: C, 54.76; H, 7.91; N, 5.94. Found: C, 54.61; H, 7.71; N, 5.90.

Synthesis of RuPNN^{HOEt}. RuPNN^{HOEt} forms rapidly and cleanly when solid **RuPNN^{HEt}** is added to ethanol or a solution of ethanol in pentane, benzene or toluene at room temperature. **RuPNN^{HOEt}** was characterized by NMR spectroscopy in solution by dissolving **RuPNN^{HEt}** (30 mg, 0.071 mmol) in toluene-d_8 (0.600 mL) containing ethanol (0.020 mL, 0.34 mmol). Rapid evolution of hydrogen gas was observed, and ^{1}H NMR spectroscopy immediately after preparation showed the formation of one species assigned as **RuPNN^{HOEt}**. Detailed NMR characterization was conducted at room temperature in C_6D_6. At room temperature, bound ethoxide, the N-H, and one of the CH_2P hydrogens are in fast exchange with free ethanol. NMR spectra recorded over the range of -90 °C to 20 °C, in toluene-d_8 showed the decoalescence of these resonances (See Supporting Information for spectral images). ^{1}H NMR (C_6D_6, 25 °C): δ 6.92 (t, 1H, $^3J_{HH}$ = 7.9 Hz, CH_{pyr}); 6.78 (d, 1H, $^3J_{HH}$ = 7.8 Hz, CH_{pyr}); 6.41 (d, 1H, $^3J_{HH}$ = 7.7 Hz, CH_{pyr}); 3.84 (br s, free EtO*H*); 3.78 (dd, 1H, $^2J_{HH}$ = 16.1 Hz, $^4J_{PH}$ = 3.7 Hz, pyrC*H*$_2$N); 3.53 (br, free CH_3CH_2OH); 3.53 (d, 1H, $^2J_{HH}$ = 16.1 Hz, pyrC*H*$_2$N); 3.07 (br d, 1H, $^2J_{HP}$ = 11.0 Hz, CH_2P); 2.97 (m, 1H, NC*H*$_2$CH$_3$); 2.84 (m, 1H, NC*H*$_2$CH$_3$);1.46 (d, 9H, $^3J_{HP}$ = 13.4 Hz, P^{t}Bu); 1.25 (t, 3H, $^3J_{HH}$ = 7.2 Hz, NCH$_2$C*H*$_3$); 1.10 (t, $^3J_{HH}$ = 7.0 Hz, free C*H*$_3$CH$_2$OH); 1.06 (d, 9H, $^3J_{HP}$ = 12.9 Hz, P^{t}Bu); –15.8 (d, $^2J_{HP}$ = 23.0 Hz, Ru-H). ^{31}P{^{1H}} NMR (C_6D_6, 25 °C): δ 105.9. ^{13}C NMR (C_6D_6, 25 °C): δ 208.7 (d, $^2J_{CP}$ = 15.8 Hz, C≡O); 162.1 (d, $^2J_{CP}$ = 4.7 Hz, C_{pyr}); 159.7 (d, $^4J_{CP}$ = 2.2 Hz, C_{pyr}); 136.3 (s, C_{pyr}); 120.5 (d, $^3J_{CP}$ = 9.0 Hz, C_{pyr}); 117.4 (s, C_{pyr}) 60.2 (s, pyr*C*H$_2$N); 58.9 (br s, free CH$_3$*C*H$_2$OH); 50.6 (s, N*C*H$_2$CH$_3$); 36.6 (d, $^1J_{CP}$ = 16.5 Hz, P*C*(CH$_3$)$_3$); 36.6 (d, $^1J_{CP}$ = 21.7 Hz, P*C*H$_2$pyr); 36.1 (d, $^1J_{CP}$ = 16.4 Hz, P*C*(CH$_3$)$_3$); 29.7 (d, $^3J_{CP}$ = 4.6 HZ, PC(*C*H$_3$)$_3$); 28.2 (d, $^3J_{CP}$ = 3.6 HZ, PC(*C*H$_3$)$_3$); 19.8 (br s, free *C*H$_3$CH$_2$OH); 14.91 (s, NCH$_2$*C*H$_3$).

The extremely high solubility of **RuPNN^{HOEt}** in polar and nonpolar solvents prevented straightforward isolation in bulk as a solid, but X-ray-quality crystals were obtained in the following manner: In the glovebox, **RuPNN^{HEt}** (20 mg, 0.047 mmol) was combined with one drop of ethanol in a small vial. Rapid evolution of hydrogen gas and the formation of a concentrated yellow solution were observed. Most of the ethanol was evaporated to leave a viscous film, after which pentane (1 mL) was added to give a yellow solution. This solution was capped loosely and allowed to slowly evaporate in the glovebox at room temperature. After one day, yellow crystals were observed, which were suitable for crystallographic characterization. Attempts to isolate the solid product obtained in this manner were not successful, as the solid was observed to decompose under vacuum, and to partly decompose giving a blue solution when washed with pentane. Dissolution of this solid in benzene-d_6 led to rapid decomposition, giving a blue solution containing several unidentified products. The solid product was stable when dissolved in benzene-d_6 containing a small amount of ethanol, and was identical by NMR to samples prepared directly from **RuPNN^{HEt}** as described above.

X-ray Crystallography, General Methods. X-ray quality crystals of **RuPNN^{H2}** and **RuPNN^{HOEt}** were grown as described in the Experimental Section. Structure determinations were performed on an Oxford Diffraction Gemini-R diffractometer, using Mo-Kα radiation at 110 K. Crystals were mounted on Hampton Research Cryoloops using Paratone-N oil. Unit cell determination, data collection and reduction, and empirical absorption correction were performed using the CrysAlisPro software package.[19] Direct methods structure solution was accomplished using SIR92,[20] and full-matrix least-squares refinement was carried out using

CRYSTALS.[21] All non-hydrogen atoms were refined anisotropically. Hydrogen atoms were placed in calculated positions, and their positions were initially refined using distance and angle restraints. All hydrogen positions were fixed in place for the final refinement cycles.

X-ray Crystallography, RuPNN^{H2}. The crystal structure of **RuPNN^{H2}** was completed as described above in the space group $P2_1/n$. Both ruthenium hydrides and the N-H hydrogen were located in the difference map and their positions were refined before being fixed in place for the final refinement cycles. A disordered molecule of toluene was present in the unit cell, located on an inversion center, which gave an occupancy of ½ toluene per asymmetric unit, compared with one molecule of **RuPNN^{H2}** per asymmetric unit. The occupancy of all atoms in the disordered toluene molecule was set to 0.5. Atom positions and displacement parameters were refined using SAME and SIMU restraints.

X-ray Crystallography, RuPNN^{HOEt}. The crystal structure of **RuPNN^{HOEt}** was completed as described above in the space group $P2_1/n$. The ruthenium hydride, N-H hydrogen, and O-H hydrogen were located in the difference map and their positions were refined before being fixed in place for the final refinement cycles.

Kinetic Studies. Kinetic experiments were conducted in an Asynt Multicell Parallel High Pressure Reactor, designed to allow sampling of aliquots from five hydrogenation reactions run in parallel. Our customization of this apparatus was described previously.[1] First, a water bath was set to 27 °C, which we determined consistently gave an internal reactor temperature of between 24.7 and 25.0 °C. The Asynt reactor was brought into the glovebox with oven-dried glass reactor liners and Teflon-coated stir bars. Reaction solutions, with a total volume of 10.0 mL, were prepared with the appropriate amount of **RuPNN^{imine}**, hexyl hexanoate, 1-hexanol, and tetradecane (0.20 equiv. relative to hexyl hexanoate) as internal standard. The reactor was closed and removed from the glovebox, and allowed to incubate for 20 minutes in the water bath. The hydrogen line was gently purged for 3 minutes, then connected to the reactor. The reactor was filled to 20 bar and vented carefully three times before being filled to the appropriate pressure and marking the start time. Aliquots were removed at predetermined times for analysis by gas chromatography. To ensure that samples represented the reaction mixture without contamination from the transfer line, 0.5 mL of reaction mixture was discarded before one drop was collected for each aliquot. The concentration of hexyl hexanoate at each time point was determined by integration of its GC signal against the tetradecane standard.

Kinetic Data Incorporated into Copasi Model. As described above, each kinetic experiment was conducted under hydrogen pressure, and aliquots were removed for analysis of the hexyl hexanoate concentration by GC, against a tetradecane internal standard. Tables S2 and S3 below show the measured concentrations of hexyl hexanoate at each time point for each experiment. Columns labeled “fitted [HH]” show the values of HH calculated with our optimized model in Copasi. As we only included time points beginning at 45 minutes in our optimizations, fitted values are only included from that point on.

Table S2. Kinetic data for varied initial concentration of **RuPNN^{imine}** and hydrogen pressure.

Variation of [RuPNN^{imine}]$_0$

$[Ru]_0$ (M)	0.0005		$[Ru]_0$ (M)	0.001		$[Ru]_0$ (M)	0.0015	
t(s)	[HH] (M)	fitted [HH]	t(s)	[HH] (M)	fitted [HH]	t(s)	[HH] (M)	fitted [HH]
0	0.2500		0	0.2500		0	0.2500	
600	0.2469		900	0.2315		720	0.2331	
1200	0.2358		1800	0.2025		1260	0.2152	
1800	0.2221		2700	0.1758	0.1758	1860	0.1915	
2700	0.2039	0.2039	3600	0.1500	0.1496	2760	0.1582	0.1582
3600	0.1860	0.1878	4800	0.1226	0.1211	3660	0.1282	0.1246
4500	0.1704	0.1731	6000	0.0993	0.0981	4560	0.1006	0.0983
5400	0.1560	0.1596	7200	0.0823	0.0795	5460	0.0787	0.0776
7200	0.1321	0.1361	9000	0.0606	0.0579	7260	0.0472	0.0481
9000	0.1127	0.1162	10800	0.0463	0.0420	9060	0.0277	0.0296
10800	0.0969	0.0992	12600	0.0345	0.0304	10860	0.0166	0.0181
12600	0.0840	0.0848	14400	0.0264	0.0219	12660	9.84E-03	1.10E-02
14400	0.0732	0.0724	16200	0.0202	0.0158			
16200	0.0646	0.0617	18000	0.0156	0.0113			

Variation of Hydrogen Pressure

P (bar)	10		P (bar)	20		P (bar)	30		P (bar)	40	
$[H_2]$ (M)	0.0383		$[H_2]$ (M)	0.0779		$[H_2]$ (M)	0.1176		$[H_2]$ (M)	0.1572	
t(s)	[HH] (M)	fitted [HH]	t(s)	[HH] (M)	fitted [HH]	t(s)	[HH] (M)	fitted [HH]	t(s)	[HH] (M)	fitted [HH]
0	0.2500		0	0.2500		0	0.2500		0	0.2500	
2400	0.2240		660	0.2381		600	0.2353		600	0.2316	
3000	0.2142	0.2142	1200	0.2214		1200	0.2139		1200	0.1999	
3600	0.2059	0.2029	1800	0.2013		1800	0.1909		1800	0.1669	
4800	0.1899	0.1821	2700	0.1736	0.1736	2700	0.1569	0.1569	2400	0.1387	
6000	0.1724	0.1638	3600	0.1473	0.1478	3600	0.1288	0.1234	3000	0.1135	0.1135
7200	0.1570	0.1474	4500	0.1245	0.1261	4500	0.1035	0.0973	3600	0.0925	0.0918
9000	0.1363	0.1261	5400	0.1044	0.1077	5400	0.0818	0.0766	4800	0.0609	0.0599
10800	0.1178	0.1080	7200	0.0753	0.0786	7200	0.0525	0.0474	6000	0.0402	0.0389
12600	0.1021	0.0925	9000	0.0530	0.0572	9000	0.0335	0.0291	7200	0.0268	0.0251
14400	0.0885	0.0792	10800	0.0386	0.0415	10800	0.0215	0.0177	9000	0.0147	0.0129
			12600	0.0278	0.0300	12600	0.0139	0.0108	10800	8.20E-03	6.62E-03
						14400	8.80E-03	6.51E-03			

Table S3. Kinetic data for varied initial concentration of hexyl hexanoate and 1-hexanol.

Variation of [hexyl hexanoate]$_0$

$[HH]_0$ (M)	0.05		$[HH]_0$ (M)	0.0625		$[HH]_0$ (M)	0.083333	
t(s)	[HH] (M)	fitted [HH]	t(s)	[HH] (M)	fitted [HH]	t(s)	[HH] (M)	fitted [HH]
0	0.0500		0	0.0625		0	0.0833	
900	0.0290		960	0.0433		1020	0.0596	
1800	0.0120		1860	0.0253		1920	0.0375	
2700	4.39E-03	4.39E-03	2760	0.0135	0.0135	2820	0.0222	0.0222
3600	1.55E-03	1.62E-03	3660	6.39E-03	6.38E-03	3720	0.0127	0.0132
4800	4.17E-04	4.32E-04	4860	2.37E-03	2.40E-03	4920	6.36E-03	6.69E-03
6000	1.13E-04	1.16E-04	6060	8.71E-04	9.09E-04	6120	3.14E-03	3.41E-03
7200	3.12E-05	3.11E-05	7260	3.26E-04	3.45E-04	7320	1.56E-03	1.75E-03
			9060	8.66E-05	8.12E-05	9120	5.54E-04	6.41E-04
						10920	1.99E-04	2.36E-04

$[HH]_0$ (M)	0.125		$[HH]_0$ (M)	0.25		$[HH]_0$ (M)	0.5		$[HH]_0$ (M)	0.75	
t(s)	[HH] (M)	fitted [HH]	t(s)	[HH] (M)	fitted [HH]	t(s)	[HH] (M)	fitted [HH]	t(s)	[HH] (M)	fitted [HH]
0	0.1250		0	0.2500		0	0.5000		0	0.7500	
1080	0.0978		1140	0.2260		600	0.4867		660	0.7422	
1980	0.0738		2040	0.1998		1200	0.4623		1260	0.7240	
2880	0.0532	0.0532	2940	0.1744	0.1744	1800	0.4302		1860	0.7029	
3780	0.0383	0.0382	3840	0.1513	0.1484	2700	0.3942	0.3942	2760	0.6746	0.6746
4980	0.0257	0.0248	5040	0.1252	0.1201	3600	0.3579	0.3642	3660	0.6452	0.6397
6180	0.0167	0.0162	6240	0.1034	0.0974	4500	0.3259	0.3364	4560	0.6118	0.6068
7380	0.0109	0.0106	7440	0.0844	0.0789	5400	0.2947	0.3107	5460	0.5804	0.5755
9180	5.96E-03	5.66E-03	9240	0.0632	0.0574	7200	0.2421	0.2646	7260	0.5177	0.5173
10980	3.74E-03	3.02E-03	11040	0.0486	0.0416	9000	0.1963	0.2245	9060	0.4536	0.4641
12780	2.76E-03	1.61E-03	12840	0.0351	0.0301	10800	0.1611	0.1897	10860	0.3974	0.4152
14580	1.03E-03	8.58E-04	14640	0.0270	0.0217	12600	0.1321	0.1595	12660	0.3385	0.3702

Variation of [hexanol]$_0$

$[HA]_0$ (M)	0.25		$[HA]_0$ (M)	0.5		$[HA]_0$ (M)	0.75		$[HA]_0$ (M)	1	
t(s)	[HH] (M)	fitted [HH]	t(s)	[HH] (M)	fitted [HH]	t(s)	[HH] (M)	fitted [HH]	t(s)	[HH] (M)	fitted [HH]
0	0.2500		0	0.2500		0	0.2500		0	0.2500	
960	0.2413		1020	0.2393		1080	0.2396		1140	0.2430	
1860	0.2272		1920	0.2238		1980	0.2282		2040	0.2300	
2760	0.2099	0.2099	2820	0.2067	0.2067	2880	0.2135	0.2135	2940	0.2185	0.2185
3660	0.1918	0.1888	3720	0.1891	0.1898	3780	0.1980	0.1982	3840	0.2043	0.2042
4860	0.1674	0.1638	4920	0.1668	0.1692	4980	0.1787	0.1792	5040	0.1876	0.1863
6060	0.1446	0.1418	6120	0.1457	0.1505	6180	0.1599	0.1617	6240	0.1698	0.1696
7260	0.1234	0.1226	7320	0.1270	0.1335	7380	0.1417	0.1456	7440	0.1533	0.1541
9060	0.0961	0.0981	9120	0.1030	0.1111	9180	0.1182	0.1240	9240	0.1310	0.1330
10860	0.0745	0.0781	10920	0.0830	0.0921	10980	0.0979	0.1051	11040	0.1111	0.1144
12660	0.0573	0.0619	12720	0.0668	0.0759	12780	0.0805	0.0887	12840	0.0941	0.0980
14460	0.0445	0.0489	14520	0.0537	0.0624	14580	0.0667	0.0746	14640	0.0786	0.0837
16260	0.0344	0.0384	16320	0.0432	0.0511	16380	0.0552	0.0625	16440	0.0666	0.0713
18060	0.0270	0.0301	18120	0.0349	0.0417	18180	0.0454	0.0523	18240	0.0561	0.0605

Kinetic Model. In the program Copasi,[22] we developed a model for the reaction network shown in Figure 11 in the main text. The file "model.cps", provided with the Supporting Information, includes the all of these species and the reactions connecting them, a function for estimating the activity coefficient of 1-hexanol from its molarity as described below, and global quantities representing the relative standard-state free energies of **a2**, **f2-g2-TS**, **g**, **g1**, **g2**, **m-n-TS**, and **m1-n1-TS**. The reactions specified in our model are shown in Scheme S1.

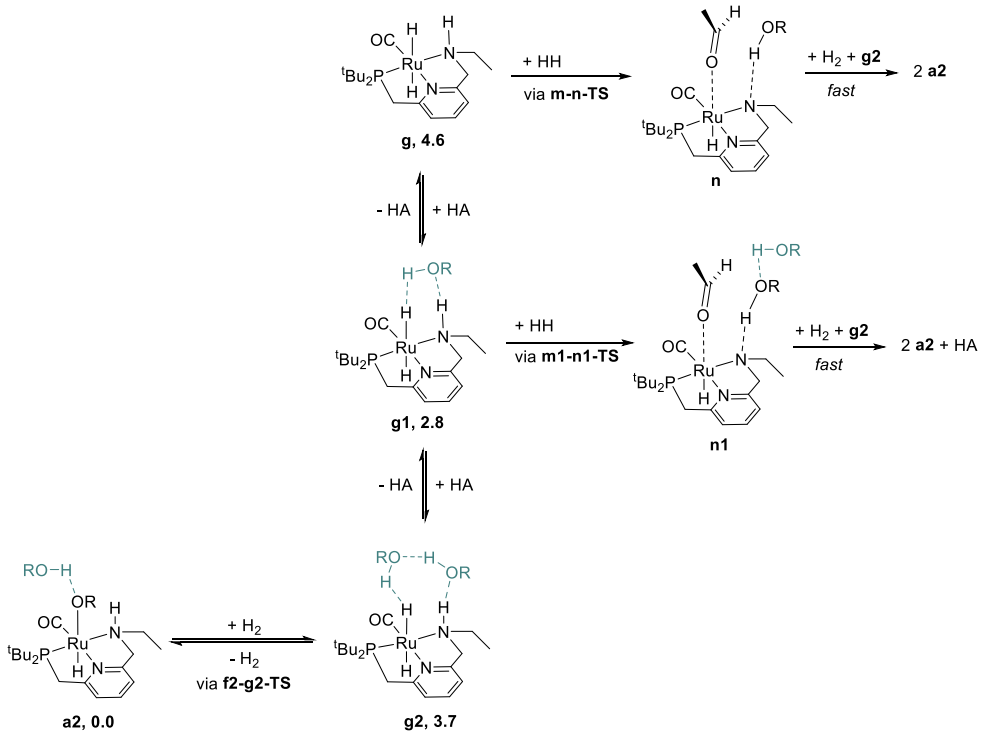

Scheme S1. Reactions specified in the Copasi model "model.cps"

Rate constants for reactions connected by **f2-g2-TS, m-n-TS**, and **m1-n1-TS** were calculated at 298.15 K from the activation free energies using the Eyring equation, taking the transmission coefficient κ as equal to one:

$$k = \frac{\kappa k_B T}{h} e^{-\left(\frac{\Delta G^{\ddagger}}{RT}\right)}$$

Reactions between **g2**, **g1**, and **g** without a calculated barrier were assumed to be in rapid equilibrium: the reverse rate constant was set at 1 x 10^{10} $M^{-1}s^{-1}$ and the forward rate constant was calculated based on the thermodynamic relationship between K_{eq} and $\Delta G°$:

$$k_{fwd} = K_{eq} k_{rev} = e^{-\left(\frac{\Delta G°}{RT}\right)} k_{rev}$$

The products of C-O cleavage were specified as **n** and **n1** in the model, formed irreversibly through **m-n-TS** and **m1-n1-TS**, respectively. In order to complete the stoichiometry of a catalytic turnover, we implemented fast (k = 1.0 x 10^{10}) reactions from **n** and **n1**, which consumed one H_2 molecule and one **g2**, and produced two **a2** molecules. For **n1**, an additional molecule of hexanol must be released as well. The additional conversion of **g2** to **a2** is necessary because two equivalents of hydrogen are consumed in each complete turnover, so the overall rate of hydrogen activation must be twice the rate of ester hydrogenolysis.

The activity coefficient of 1-hexanol in toluene as a function of its molarity was estimated with a model developed by Li and coworkers, which uses the concentration dependence of NMR chemical shifts to

predict activity coefficients as a function of composition.[23] The data were fit well with the following equation, where c is the molarity of hexanol and $\gamma_{hexanol}$ is its activity coefficient. This equation was used to calculate the activity coefficient of hexanol in our Copasi model as a function of its transient concentration at each time point. For all reaction steps incorporating a molecule of hexanol, we multiplied the rate constant calculated above by $\gamma_{hexanol}$.

$$\gamma_{hexanol} = 4.070\, e^{-\frac{c}{1.700}} + 3.812\, e^{-\frac{c}{0.4177}} + 0.9710$$

Importantly, because rate constants are calculated dynamically in our model from the relative standard-state free energies of the species, it is possible to adjust the energies to examine qualitatively the effect on the reaction time course, and to execute a Parameter Estimation task where selected energies are optimized to fit the kinetic data. The included file "data.txt" contains the kinetic data from the 18 experiments used in the global fit, in the format directly readable by Copasi.

We obtained the optimal fit to the kinetic data by allowing the relative standard-state free energies of **f2-g2-TS**, **m1-n1-TS**, and **m-n-TS** to vary, while holding the free energies of **a2**, **g2**, **g1**, and **g** constant at the values calculated by DFT (see Figure 16). In the fitting process, it was essential to use the "Value Scaling" option for weighting of the residual errors as the minimized objective function, rather than minimizing the mean or mean-square of errors, to ensure that the data at very low [hexyl hexanoate] received sufficient weight. In order to confirm that the solution we obtained corresponded to the global minimum of weighted error, we repeated the fitting process ten times using an evolutionary programming algorithm, each time choosing randomized start values within ± 10 kcal/mol of the DFT values for each of the three optimized free energies, and found that the energies converged to the same values each time. We note that the standard deviations of the fitted free energies appear very small, in the range of 0.01 to 0.02 kcal/mol. These small errors arise from the logarithmic relationship of activation barriers to their associated rate constants: for example, at 298.15 K an error of 0.020 kcal/mol in the free-energy barrier translates to a 3.5% error in the associated rate constant.

Kinetic Data with Added Isopropyl Alcohol. As described in the main text, we conducted a series of experiments demonstrating that, although added 1-hexanol inhibits turnover, added isopropyl alcohol accelerates turnover. The concentration data plotted in Figure 13 in the main text is provided in Table S4 below.

Table S4. Kinetic data with added isopropyl alcohol.[a]

[iPrOH] (M)	0.00	[iPrOH] (M)	0.25	[iPrOH] (M)	0.50	[iPrOH] (M)	0.75
t(s)	[HH] (M)	t(s)	[HH] (M)	t(s)	[HH] (M)	t(s)	[HH] (M)
0	0.2500	0	0.2500	0	0.2500	0	0.2500
660	0.2381	720	0.2243	780	0.2183	840	0.2175
1200	0.2214	1320	0.1987	1380	0.1920	1440	0.1868
1800	0.2013	1920	0.1700	1980	0.1638	2040	0.1585
2700	0.1736	2820	0.1364	2880	0.1275	2940	0.1181
3600	0.1473	3720	0.1093	3780	0.0979	3840	0.0861
4500	0.1245	4620	0.0860	4680	0.0740	4740	0.0622
5400	0.1044	5520	0.0679	5580	0.0550	5640	0.0437
7200	0.0753	7320	0.0419	7380	0.0300	7440	0.0219
9000	0.0530	9120	0.0249	9180	0.0166	9240	0.0108
10800	0.0386	10920	0.0155	10980	0.0092	11040	0.0055
12600	0.0278	12720	0.0096	12780	0.0053	12840	0.0030

[a]The first column with no added isopropyl alcohol was duplicated from Table S2.

References

(1) He, T.; Buttner, J. C.; Reynolds, E. F.; Pham, J.; Malek, J. C.; Keith, J. M.; Chianese, A. R. *J. Am. Chem. Soc.* 2019, **141**, 17404-17413.

(2) Frisch, M. J.; Trucks, G. W.; Schlegel, H. B.; Scuseria, G. E.; Robb, M. A.; Cheeseman, J. R.; Scalmani, G.; Barone, V.; Petersson, G. A.; Nakatsuji, H.; Li, X.; Caricato, M.; Marenich, A. V.; Bloino, J.; Janesko, B. G.; Gomperts, R.; Mennucci, B.; Hratchian, H. P.; Ortiz, J. V.; Izmaylov, A. F.; Sonnenberg, J. L.; Williams; Ding, F.; Lipparini, F.; Egidi, F.; Goings, J.; Peng, B.; Petrone, A.; Henderson, T.; Ranasinghe, D.; Zakrzewski, V. G.; Gao, J.; Rega, N.; Zheng, G.; Liang, W.; Hada, M.; Ehara, M.; Toyota, K.; Fukuda, R.; Hasegawa, J.; Ishida, M.; Nakajima, T.; Honda, Y.; Kitao, O.; Nakai, H.; Vreven, T.; Throssell, K.; Montgomery Jr., J. A.; Peralta, J. E.; Ogliaro, F.; Bearpark, M. J.; Heyd, J. J.; Brothers, E. N.; Kudin, K. N.; Staroverov, V. N.; Keith, T. A.; Kobayashi, R.; Normand, J.; Raghavachari, K.; Rendell, A. P.; Burant, J. C.; Iyengar, S. S.; Tomasi, J.; Cossi, M.; Millam, J. M.; Klene, M.; Adamo, C.; Cammi, R.; Ochterski, J. W.; Martin, R. L.; Morokuma, K.; Farkas, O.; Foresman, J. B.; Fox, D. J. *Gaussian 16 Rev. B.01*, Wallingford, CT, 2016.

(3) (a) Lee, C.; Yang, W.; Parr, R. G. *Phys. Rev. B* 1988, **37**, 785-789. (b) Becke, A. D. *J. Chem. Phys.* 1993, **98**, 5648-5652.

(4) Hay, P. J.; Wadt, W. R. *J. Chem. Phys.* 1985, **82**, 299-310.

(5) Ehlers, A.; Böhme, M.; Dapprich, S.; Gobbi, A.; Höllwarth, A.; Jonas, V.; Köhler, K.; Stegmann, R.; Veldkamp, A.; Frenking, G. *Chem. Phys. Lett.* 1993, **208**, 111-114.

(6) Roy, L. E.; Hay, P. J.; Martin, R. L. *J. Chem. Theory Comput.* 2008, **4**, 1029-1031.

(7) (a) Krishnan, R.; Binkley, J. S.; Seeger, R.; Pople, J. A. *J. Chem. Phys.* 1980, **72**, 650-654. (b) McLean, A. D.; Chandler, G. S. *J. Chem. Phys.* 1980, **72**, 5639-5648.

(8) Marenich, A. V.; Cramer, C. J.; Truhlar, D. G. *J. Phys. Chem. B* 2009, **113**, 6378-6396.

(9) Dub, P. A.; Gordon, J. C. *Dalton Trans.* 2016, **45**, 6756-6781.

(10) (a) Zweifel, T.; Naubron, J. V.; Buttner, T.; Ott, T.; Grützmacher, H. *Angew. Chem. Int. Ed.* 2008, **47**, 3245-3249. (b) Zweifel, T.; Naubron, J. V.; Grützmacher, H. *Angew. Chem. Int. Ed.* 2009, **48**, 559-563. (c) Prokopchuk, D. E.; Morris, R. H. *Organometallics* 2012, **31**, 7375-7385.

(11) Cramer, C. J., In *Essentials of Computational Chemistry*, 2nd ed.; Wiley: Chichester, UK, 2004; 378-379.

(12) (a) Zhao, Y.; Truhlar, D. G. *Theor. Chem. Acc.* 2007, **120**, 215-241. (b) Zhao, Y.; Truhlar, D. G. *Acc. Chem. Res.* 2008, **41**, 157-167.
(13) Hasanayn, F.; Baroudi, A. *Organometallics* 2013, **32**, 2493-2496.
(14) Li, H.; Wang, X.; Huang, F.; Lu, G.; Jiang, J.; Wang, Z.-X. *Organometallics* 2011, **30**, 5233-5247.
(15) Wang, H.; Liu, C.; Zhang, D. *Mol. Catal.* 2017, **440**, 120-132.
(16) Gusev, D. G. *Organometallics* 2020, **39**, 258-270.
(17) Martin, R. L.; Hay, P. J.; Pratt, L. R. *J. Phys. Chem. A* 1998, **102**, 3565-3573.
(18) Yu, Z.-X.; Houk, K. N. *J. Am. Chem. Soc.* 2003, **125**, 13825-13830.
(19) Oxford Diffraction (2007). Oxford Diffraction Ltd., Xcalibur Ccd System, Crysalispro Software System, Version 1.171.32.
(20) Altomare, A.; Cascarano, M.; Giacovazzo, C.; Guagliardi, A.; Burla, M. C.; Polidori, G.; Camalli, M. *J. Appl. Cryst.* 1994, **27**, 435-436.
(21) Betteridge, P. W.; Carruthers, J. R.; Cooper, R. I.; Prout, K.; Watkin, D. J. *J. Appl. Cryst.* 2003, **36**, 1487.
(22) Hoops, S.; Sahle, S.; Gauges, R.; Lee, C.; Pahle, J.; Simus, N.; Singhal, M.; Xu, L.; Mendes, P.; Kummer, U. *Bioinformatics* 2006, **22**, 3067-3074.
(23) Xu, Y.; Li, H.; Wang, C.; Ma, L.; Han, S. *Ind. Eng. Chem. Res.* 2005, **44**, 408-415.

NMR Spectra of RuPNN^{HOEt}

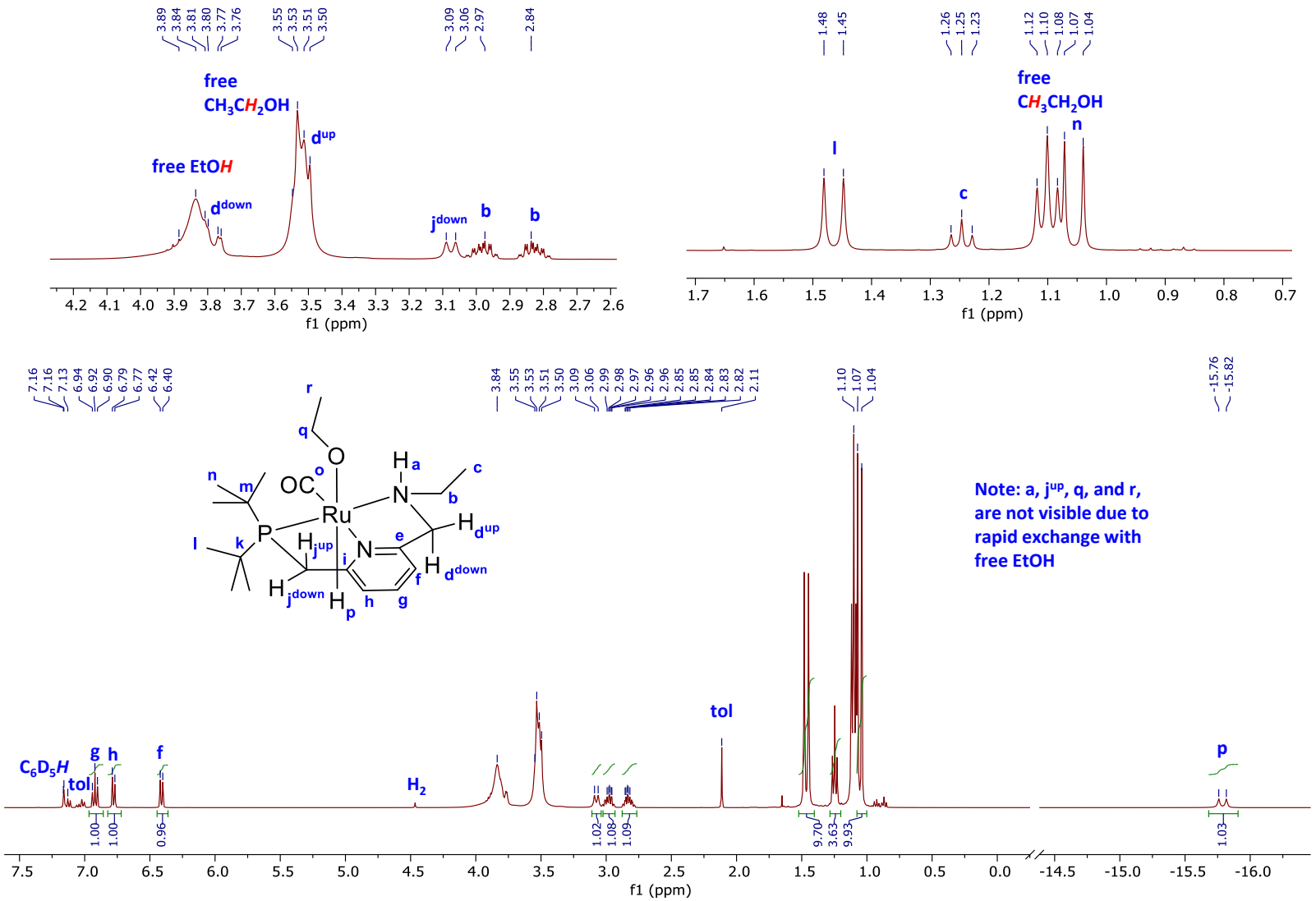

Figure S20. ^{1}H NMR spectrum (C_6D_6, room temperature) of **RuPNN^{HOEt}**, prepared in situ from **RuPNN^{HEt}** and ethanol.

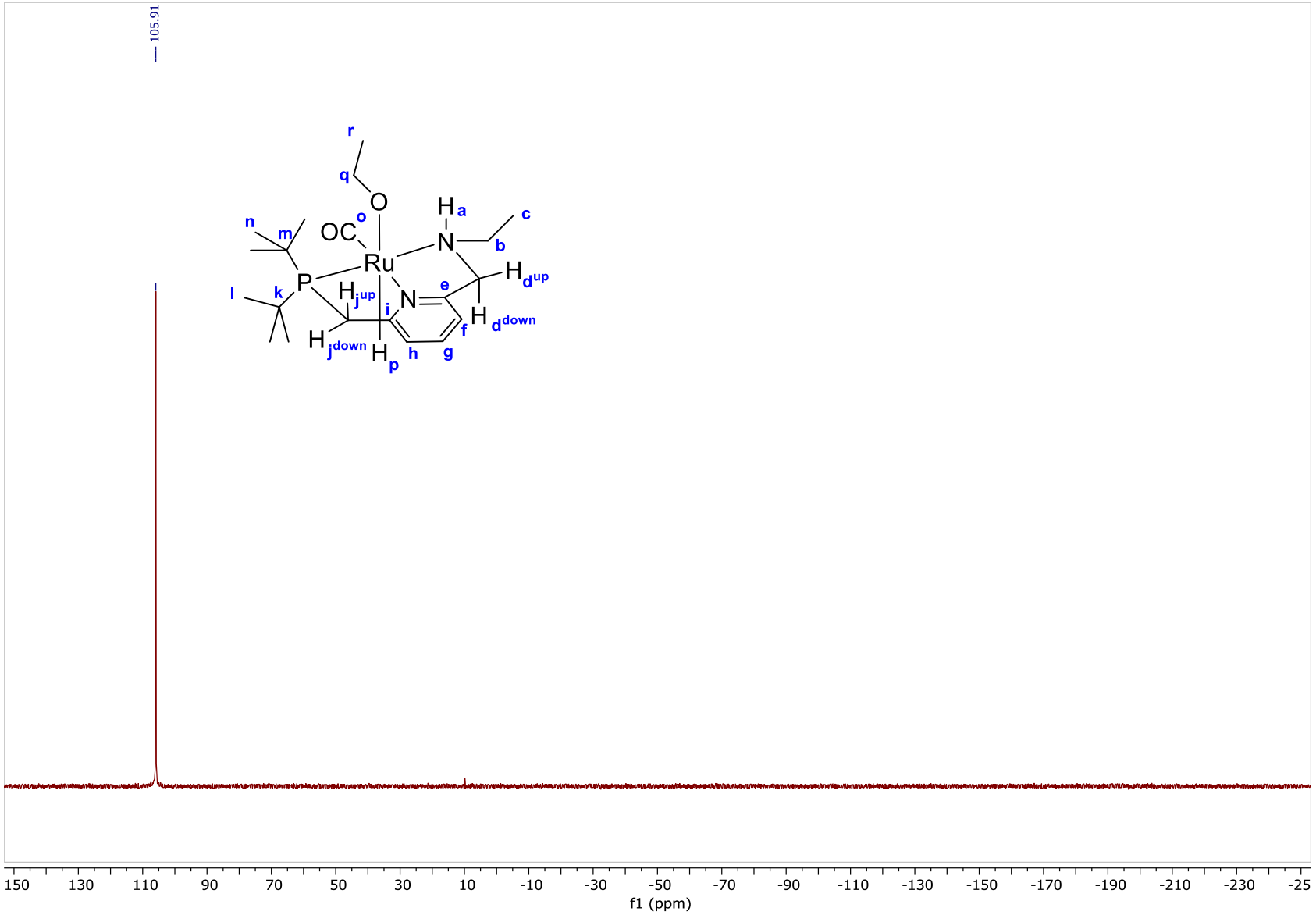

Figure S21. $^{31}P\{^{1}H\}$ NMR spectrum (C_6D_6, room temperature) of **RuPNN^{HOEt}**, prepared in situ from **RuPNN^{HEt}** and ethanol.

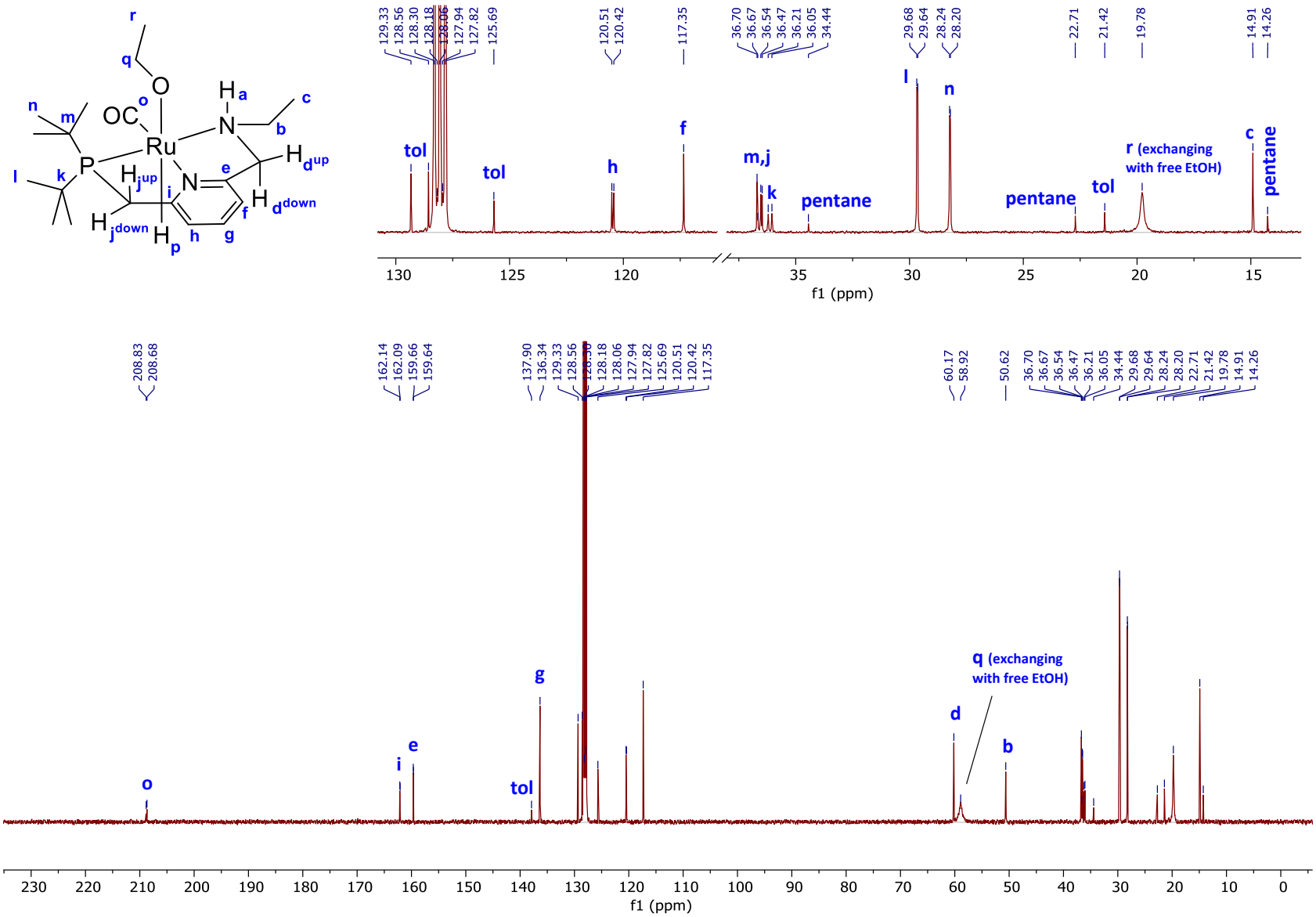

Figure S22. $^{13}C\{^{1}H\}$ NMR spectrum (C_6D_6, room temperature) of **RuPNN^{HOEt}**, prepared in situ from **RuPNN^{HEt}** and ethanol.

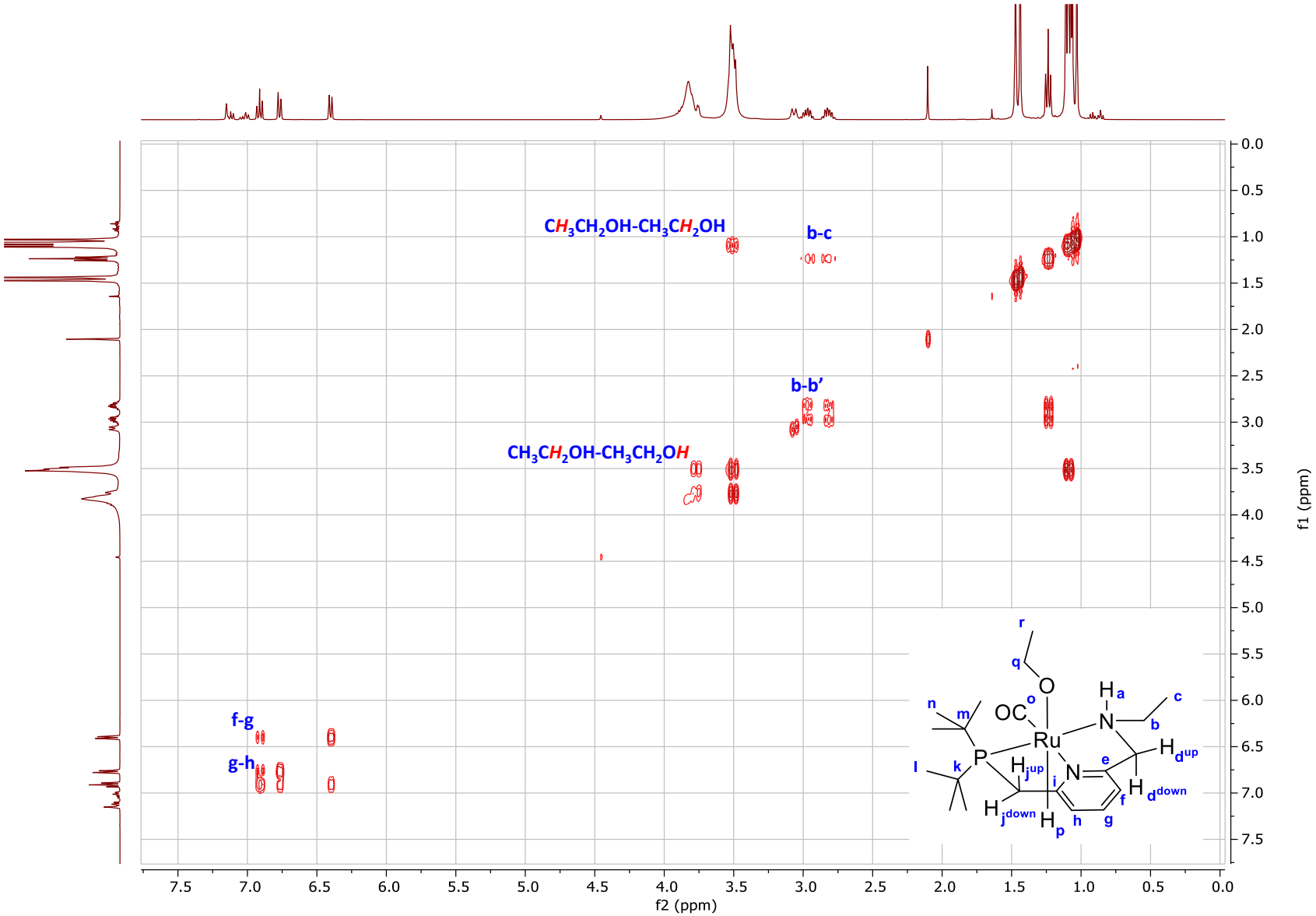

Figure S23. COSY (C_6D_6, room temperature) of **RuPNN^{HOEt}**, prepared in situ from **RuPNN^{HEt}** and ethanol.

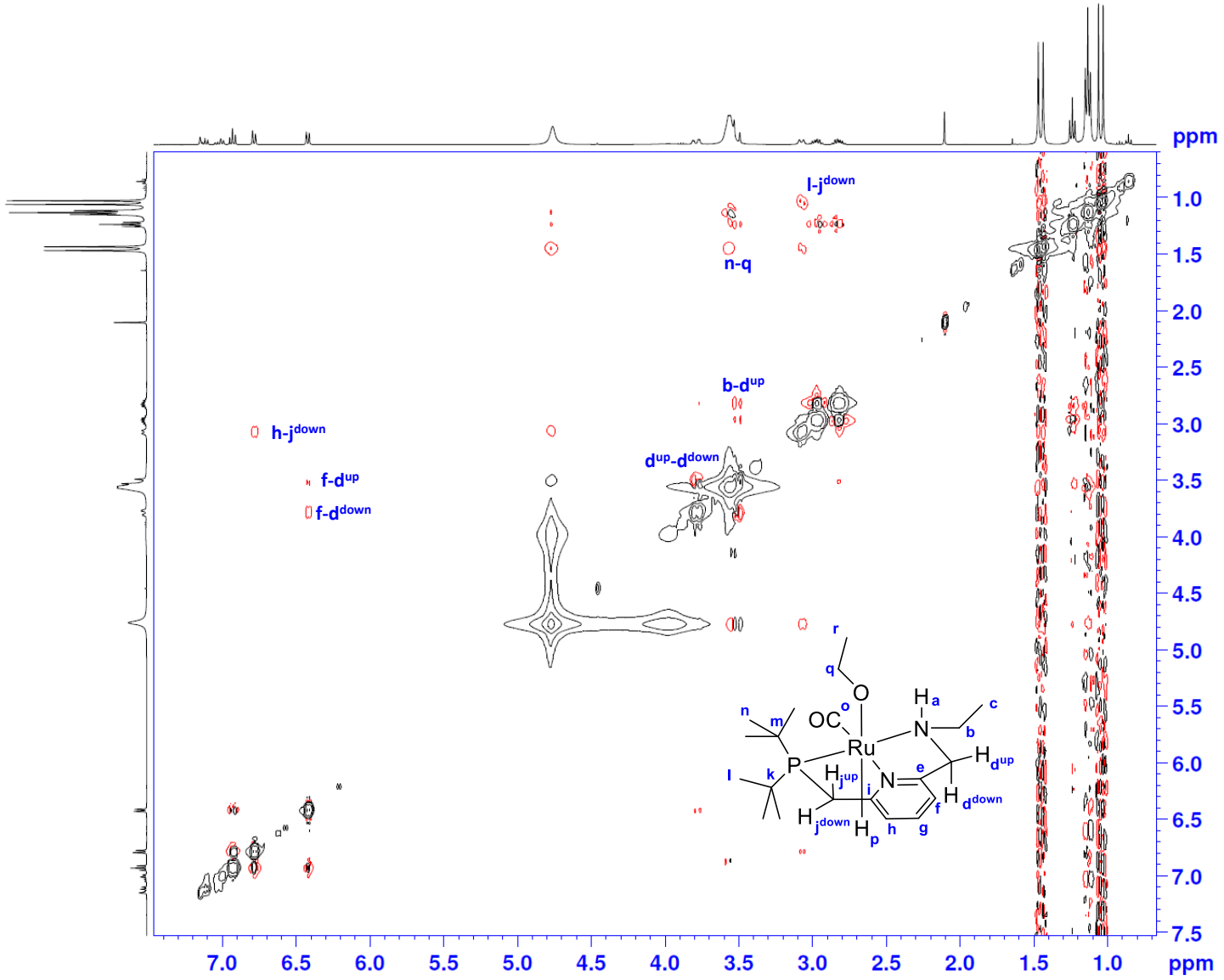

Figure S24. NOESY (C_6D_6, room temperature) of **RuPNN^{HOEt}**, prepared in situ from **RuPNN^{HEt}** and ethanol.

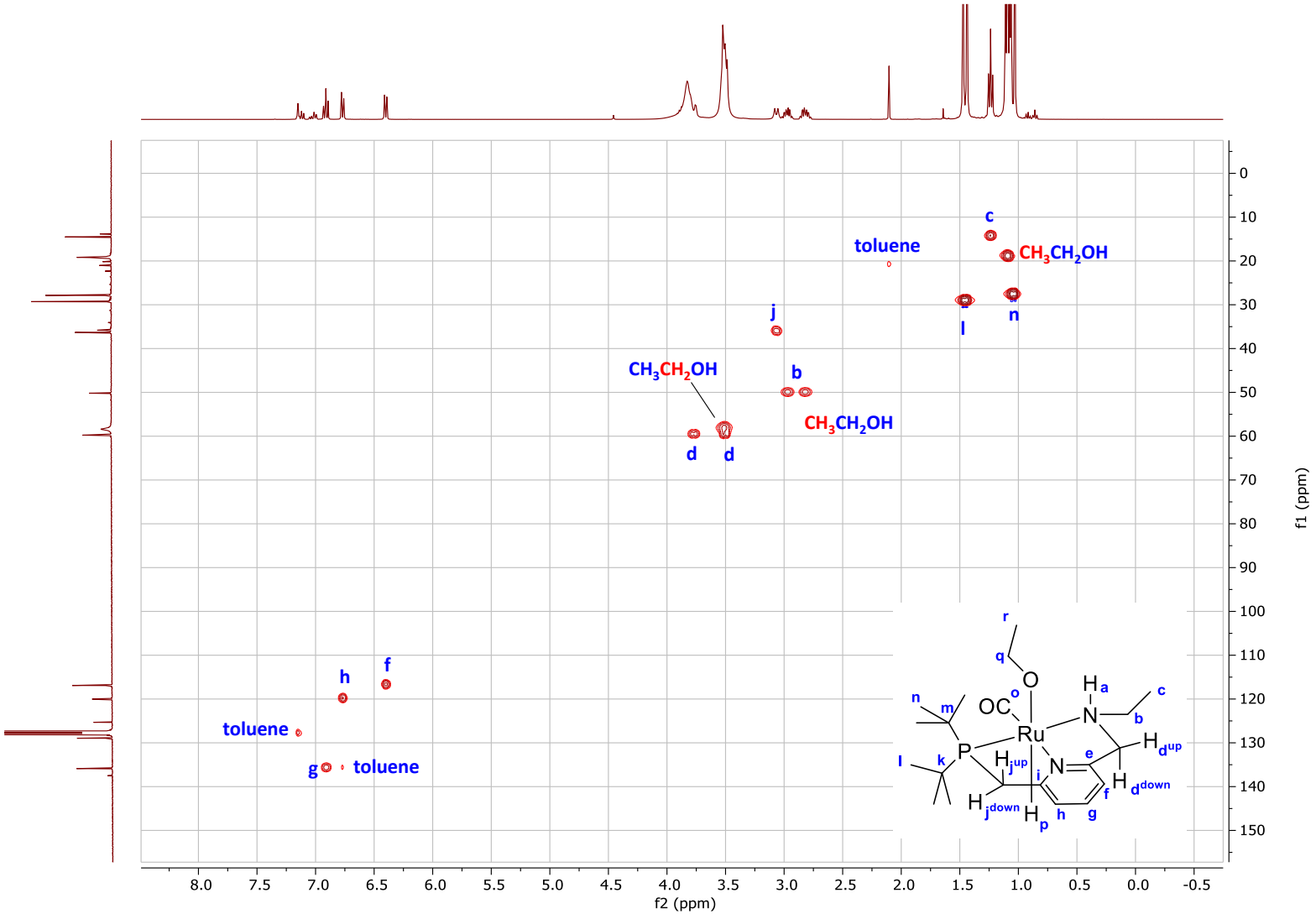

Figure S25. HSQC spectrum (C_6D_6, room temperature) of **RuPNN^{HOEt}**, prepared in situ from **RuPNN^{HEt}** and ethanol.

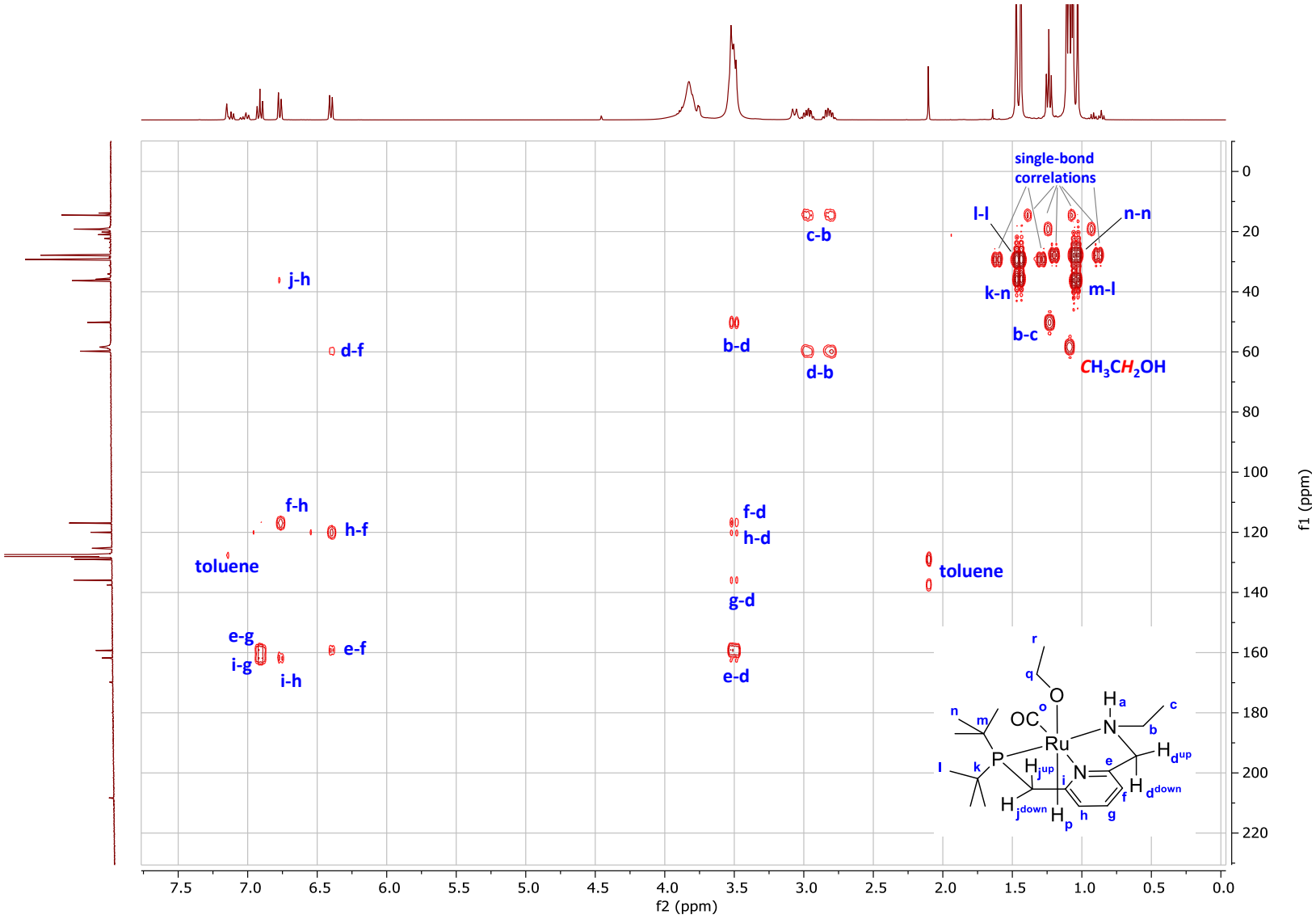

Figure S26. HMBC spectrum (C_6D_6, room temperature) of **RuPNN^{HOEt}**, prepared in situ from **RuPNN^{HEt}** and ethanol. Cross-peaks are labeled as **x-y**, where **x** is the carbon and **y** is the hydrogen giving rise to the signal.

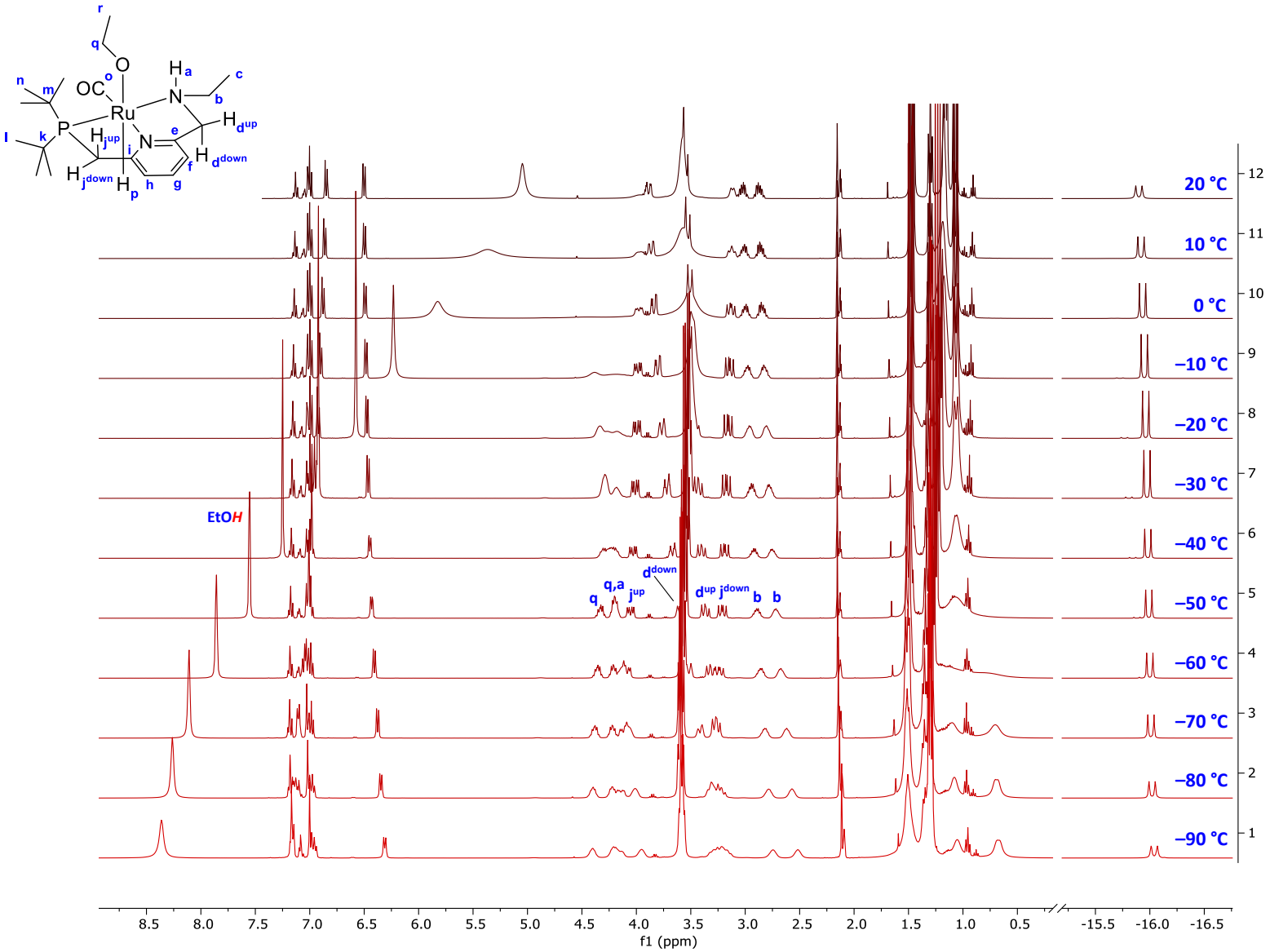

Figure S27. Variable-temperature ^{1}H NMR spectra (toluene-d_8) of **RuPNN^{HOEt}**, prepared in situ from **RuPNN^{HEt}** and ethanol.